EUROPEAN ORGANIZATION FOR NUCLEAR RESEARCH

Apparatus for Meson and Baryon Experimental Research

CERN-SPSC-2022-023
SPSC-SR-313
May 30, 2022

AMBER Status Report 2022

The AMBER Collaboration

Abstract

The report reviews the activities and the achievements of the Collaboration towards the current date. Covered items are the results and ongoing analysis for the studies, collected data so far and the preparations for the future runs for the measurements of the Proton Charge-Radius, the Anti-Proton Cross-Section and Drell Yan process.

Contents

1 Introduction **2**

2 Proton Charge-Radius Measurement **3**

2.1 Test Run in 2018 and 2021 . . . 3

2.1.1 Further Results from the 2018 Test Run . . . 4

2.1.2 Preliminary Results from the 2021 Pilot Run . . . 5

2.2 Ongoing Activities and Plans for 2022 . . . 12

2.3 Plans for 2023 . . . 12

2.4 Perspectives for Hadron Radii Measured in Inverse Kinematics . . . 14

3 Anti-Proton Production Cross-Section Measurements **15**

3.1 Full MC Simulation of the Anti-Protons Experimental Setup . . . 15

3.2 Study of the COMPASS RICH PID efficiency and purity . . . 16

3.3 Hadron Beam Test at the M2 Beam Line . . . 17

3.4 Plans for 2022 and 2023 . . . 18

4 Meson structure measurement **18**

4.1 Shielding and radio protection limitations . . . 19

4.2 Track and vertex reconstruction . . . 20

4.3 Possibility for kaon structure studies . . . 21

4.4 Plans for 2023 . . . 22

5 Hardware **23**

5.1 TPC and Gas System . . . 23

5.2 Unified Tracking Station . . . 23

5.2.1 Scintillating Fiber Hodoscope . . . 24

5.2.2 Silicon Pixel Detector . . . 26

5.3 DAQ . . . 27

6 Publications, presentations to conferences and collaboration matters **28**

References 30

1 Introduction

The report describes the status and results towards the current date for the upcoming projects of the proton charge-radius measurement, the anti-proton production cross-sections measurement, the Drell-Yan process and their respective developments in hardware and organisation.

2 Proton Charge-Radius Measurement

We present the recent developments for the proton charge-radius measurement (PRM) with high-energetic muons at the M2 beam line within the scope of the AMBER collaboration as described in the initial proposal [1] presented to the SPSC in 2019. As motivation for the PRM in this proposal a prior feasibility test run in 2018 was performed. A prototype TPC (ACTAF2) combined with silicon tracking detectors showed the capability of combined muon and recoil proton measurement in the elastic-scattering kinematics. Additional results of this analysis will be presented. The second step towards the PRM program was the pilot run recommended by the SPSC [2], if successful [3], as preparation for a main physics run. The proposed pilot run was performed in October 2021 in the M2 test-beam area using the so-called IKAR TPC as a down-scaled version of the planned main TPC. This TPC consists of two drift chambers and is equipped with an adapted readout-plane structure developed especially for the recoil-proton measurement in the muon beam. Analysis is in progress and preliminary results will be presented below. Developments for the Unified Tracking Station (UTS) are ongoing and two beam tests are foreseen for May and October this year. Whereas the first beam time is dedicated to study the scintillating fibers used in the UTS and will take place in a parasitic operation mode at the M2 beam dump location during the COMPASS data taking, the second test will be located directly in the COMPASS target region with close-to-final beam properties to study the full UTS setup and evaluate its performance in a later analysis. Due to the overall changes in the beam time schedule the PRM measurement could take place earliest in the second half of 2023. Due to difficulties in obtaining the required electronics and the restrictions of Russian participation studies are ongoing towards a reduced setup for the PRM with the spectrometer. Anticipated time lines of the UTS project and a possible beam time schedule in 2022/2023 are shown in Fig. 1.

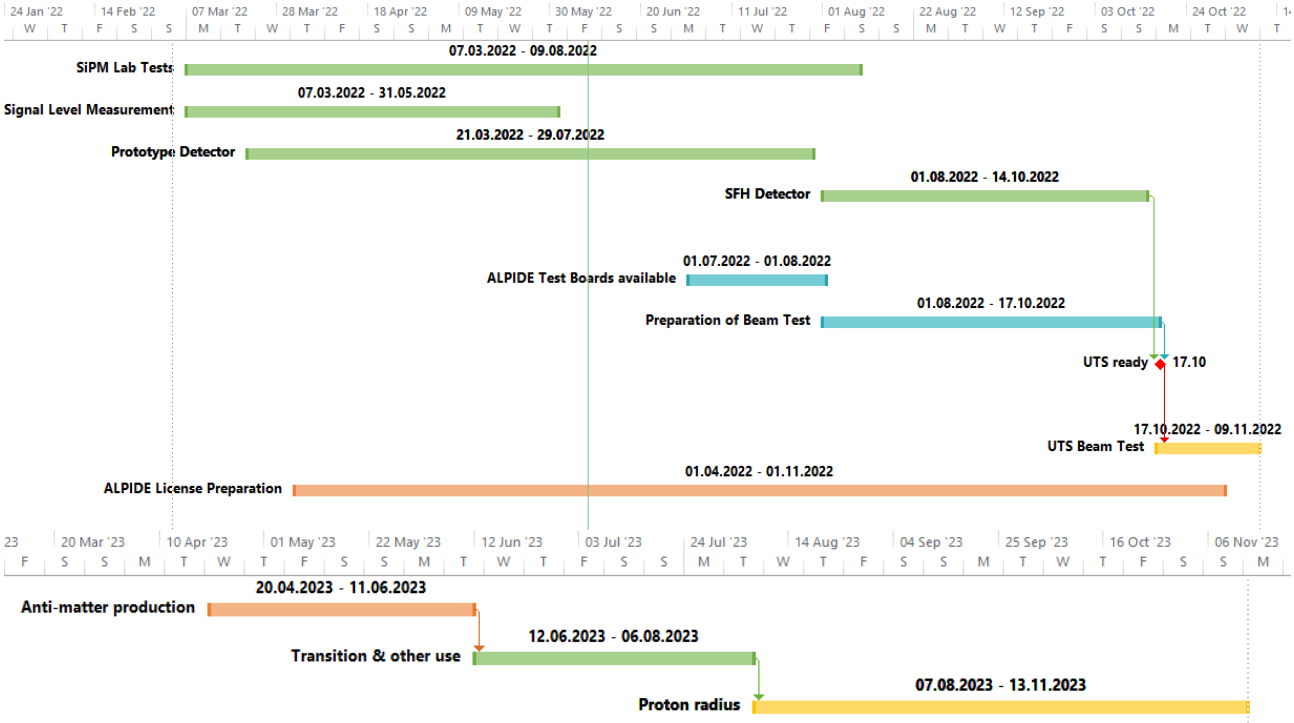

Fig. 1: Timelines for the UTS projects (SFH and SPD) including foreseen beam tests in 2022 (top). Anticipated time lines for a possible PRM beam time in 2023 (bottom).

2.1 Test Run in 2018 and 2021

As preparation for the measurement of the proton charge-radius a first test in 2018 and a pilot run in 2021 were performed. The parasitic test run in 2018 served as feasibility test for the layout of the overall setup of the measurement principle and was the basis of the initial proposal for the AMBER PRM project. Experiences and results of this test run served as input for studies, simulations and design of the final layout for the PRM setup. In 2021, a dedicated 20-days beam time was used to evaluate the performance of a close-to-final setup at the

test beam location [4]. In the following, additional results from the 2018 test run and preliminary results from the ongoing analysis of the 2021 pilot run are presented.

2.1.1 *Further Results from the 2018 Test Run*

A test run prior to the initial proposal was performed in 2018. This test run was used as a proof-of-principle measurement to combine the measurement of recoil protons in a TPC detector and of scattered muons with tracking detectors in a fixed-target experiment, for evaluating the capability to achieve a complete measurement of the elastic muon-proton kinematics. The preliminary results on muon and proton correlations shown in the proposal served as input for a more refined analysis of the data. Additional results are presented below.

The primary vertex z-distribution shown in Fig. 2(a) reassembles clearly the structures of the setup described in more detail in [1]. The TPC structures with anode and cathode surrounding the active area are visible, as well as beam window positions on the upstream and downstream side. Vertices in the two adjacent silicon tracking detectors are visible. In order to extract the vertex z-resolution, the comparable small width of the cathode structure is used. In Fig. 2(b) the parameterised vertex z-resolution for the real data is shown together with data points resulting from the Monte-Carlo simulation. Good agreement is found for the main region in the measured scattering angle. For larger scattering angles the simulation tends to slightly undershoot the data.

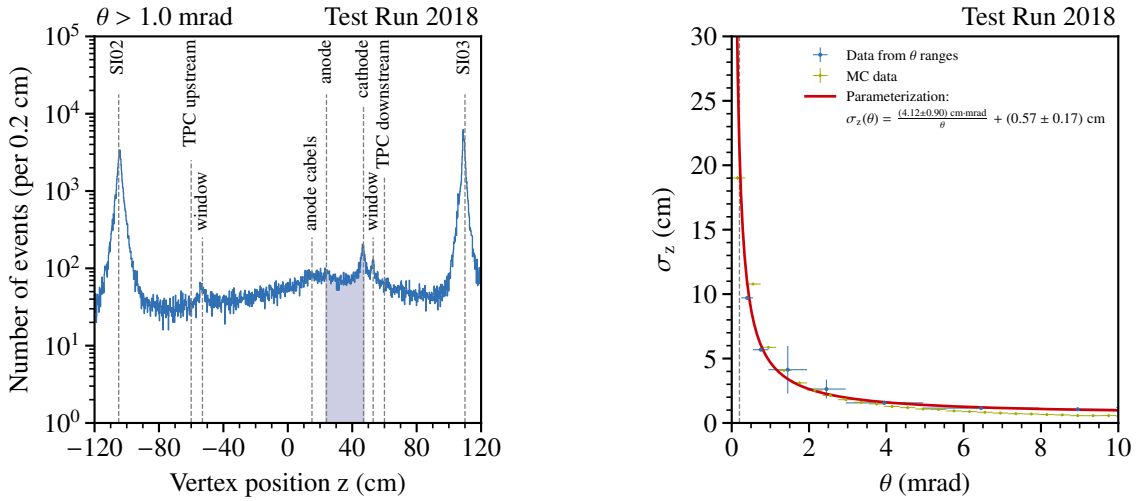

(a) (b)

Fig. 2: (a) Vertex z-distribution of the 2018 test setup. The respective structures are indicated together with the active area of the TPC marked in blue; (b) Resolution in the vertex z-position. A parameterisation for the real data is given together with a comparison to Monte-Carlo data. The dashed line indicates the lower limit in the selected scattering angle as used for the results shown in [1].

As described in the proposal, elastic muon-electron scattering is planned to be used as calibration channel for the measured beam momentum of the BMS (Beam Momentum Station), which is placed in the beam line. These kinematics have a clear angular correlation of the outgoing muon and electron tracks for respective beam momenta. A dedicated event selection to extract these events was performed, and the results are shown in Fig. 3. In Fig. 3(a) the angular correlation between the two outgoing tracks is shown. Since no particle identification was present, the distribution is mirror symmetric with respect to the (virtual) line of equal scattering angles. Using an average beam energy of 178.6 GeV/c, as extracted from Fig. 3(b), the predicted correlation for every event is indicated and also made mirror symmetric. Based on the angular correlation, the incoming beam energy can be calculated for each individual event. For the test run, this result is shown in Fig. 3(b). Since the full data

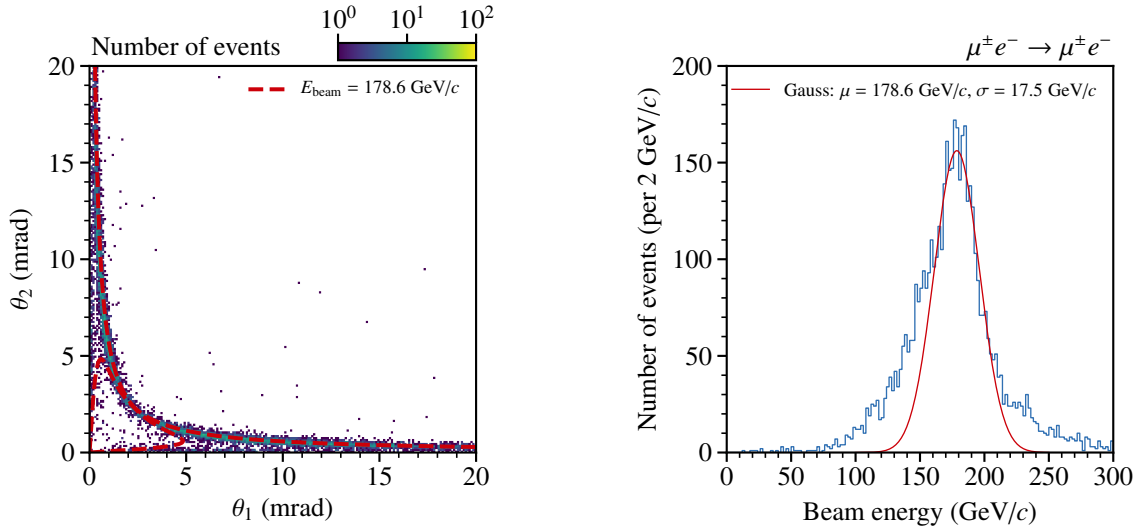

(a) (b)

Fig. 3: (a) Angular correlation between the two outgoing tracks, shown together with the prediction for a beam energy of 178.6 GeV/c; (b) Extracted beam energy.

set contains various beam settings of pure muon beam as well as resulting muons from the COMPASS Drell-Yan measurement during the parasitic data taking, the calculated beam energy exhibits a broader spectrum and is slightly down-shifted with respect to the initial 190 GeV/c beam energy. As the test setup was placed at the most downstream location of the COMPASS spectrometer, which results in a large amount of material that the beam particles had to pass, the beam energy distribution is further widened.

2.1.2 Preliminary Results from the 2021 Pilot Run

In 2021 a dedicated pilot run was performed at the M2 test beam location (CEDAR position). During 20 days of dedicated beam time a close-to-final setup was installed. This included about four days of combined data taking for TPC and tracking detectors. The main element of the setup was the so-called IKAR TPC, which represents a down-scaled version of the final TPC with two instead of four drift chambers, a slightly smaller readout pad-plane and a reduced pressure of 8 bar compared to the planned 20 bar of the final layout. For tracking, five silicon tracking detector stations were operated, two upstream and three downstream of the TPC. In addition, two scintillating fiber trackers were installed, one upstream and one downstream of the TPC. A schematic drawing of the setup is shown in Fig. 4. A triggered DAQ system was used to read out the tracking detectors. For the TPC, a dedicated DAQ system was installed, exploiting the "self-triggering" mode of the TPC. Similar as in the test run described in Sec. 2.1.1, a common timestamp was applied to synchronize the events from the two DAQ systems in the offline analysis. In order to maximize the number of clean events, so-called enrichment-trigger elements (BT01A and BT01B) were operated to select beam trajectories from the central region of the beam with low divergence. A schematic drawing is shown in Fig. 5. The triggered events are expected to also hit the central part of the segmented TPC readout plane. Furthermore, selecting the inner part of the beam allowed us to reduce the trigger rate to the maximum of 40 kHz that the DAQ system can handle. In addition, the COMPASS spectrometer including tracking detectors and calorimetry was read out together with the pilot run tracking system. This allows a momentum measurement and the usage of the electromagnetic calorimeter.

The main goals of the pilot run are to evaluate the TPC performance in a focused muon beam with the proposed rate of 2 MHz and to study the energy resolution as well as the beam-induced noise with the proposed new pad-plane structure.

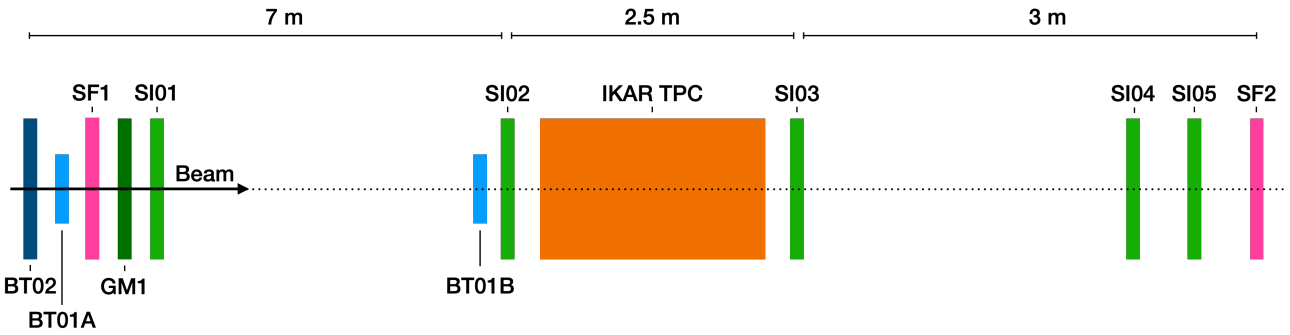

Fig. 4: Schematic drawing of the setup for the pilot run, with the beam coming from the left side. The central IKAR TPC is surrounded by silicon tracking detectors (SI01 to SI05) on the upstream and downstream side. Each side has a lever arm of about 3 m. The upstream side is equipped with enrichment beam-trigger elements (enrichment for central beam part).

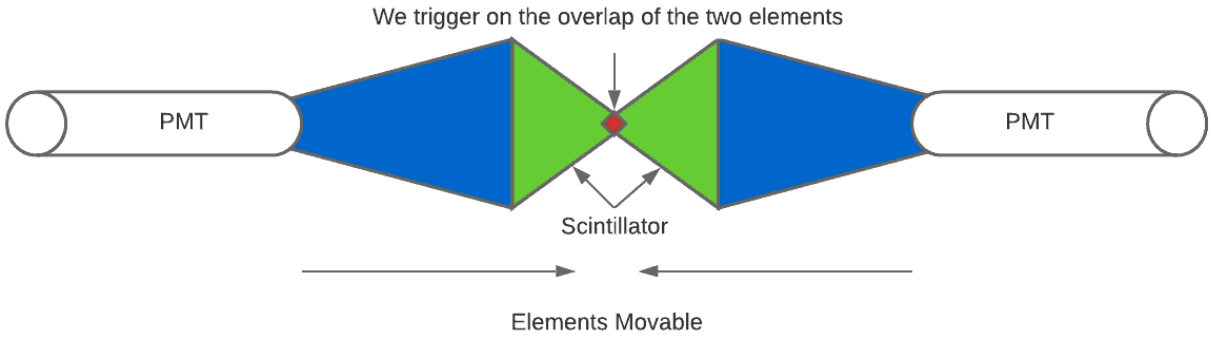

Fig. 5: Schematic drawing of the enrichment beam trigger element for the pilot run. The active scintillator parts are marked in green, with the trigger section as overlap of these elements marked in red.

A dedicated gas-system infrastructure was built and operated to guarantee the required hydrogen gas quality as well as the monitoring of the gas density parameters, i.e. T and P. The system consists of a set of bottles of pure hydrogen (6.0) at 200 bar. The pressure is reduced to 10 bar before injecting the gas into the TPC vessel. A mechanical back-pressure regulator allows for TPC pressure adjustment. The gas enters the TPC volume at a rate of 2 l/h, while an identical amout is exhausted. Water and oxygen contamination are continuously measured via dedicated sensors at the exhaust line of the TPC. A fully automated PLC operated system was deployed and successfully operated in order to guarantee the correct operational sequence of the gas system, prevent damages to the detector and respect the CERN safety requirements in case of malfunctioning of the apparatus and/or fire detection alarm. The current layout is a down-scaled version of the one needed for the main run. The same setup will be used, once upgraded, for the final TPC and gas system.

As a focused beam at a fixed beam energy of 100 GeV/c was used, a clean data sample of elastic muon-proton scattering events can be expected from the Pilot Run analysis, similar as anticipated for the final measurement. The future Pilot Run analysis will include calibration tests using information from the BMS station and from elastic muon-electron scattering events.

In total, about $3 \cdot 10^9$ tracking events and about $1.2 \cdot 10^9$ events of combined operation of TPC and tracking detectors were recorded. With the common time stamp, these events can be associated to one another, and based on the time difference correlated events can be identified as described for the 2018 Test Run data in [1].

A preliminary run-by-run alignment was performed based on only the silicon tracking detectors. The alignment will be refined further by adding the scintillating fiber detectors. At a later stage, the test beam area part will be combined with the BMS and the spectrometer. Based on this preliminary alignment the primary vertex

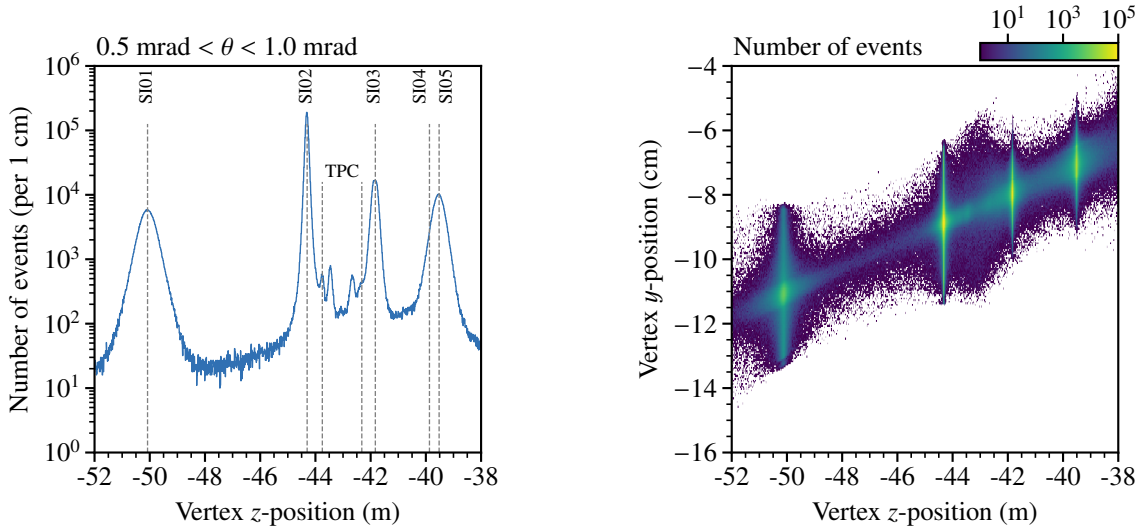

(a) (b)

Fig. 6: (a) Primary vertex z-position. Structures of the setup are visible and indicated; (b) Vertex y-position depending on the vertex z-position. The inclination of the beam line and therefore the setup is clearly visible.

distributions as shown in Fig. 6 can be extracted. In Fig. 6(a) the vertex z-position is shown. The structures of the setup, especially the inner part of the TPC, are clearly visible. Anode and cathode structures can be identified as well as the separation of the two drift cells in the center. In addition, the position of the silicon tracking detectors is visible due to hits that were wrongly assigned to tracks. This does not affect the tracking reconstruction in the central region around the TPC. As the alignment procedure is ongoing and hence still preliminary, it can be expected that these artefacts will be cured. At the current stage the silicon station SI04 is not included in the tracking. Since the pilot run setup is placed in the beam line part of the CEDAR region with an inclination of about 3.6 mrad, the vertex y-distribution along the setup exhibits a similar behaviour, as shown in Fig. 6(b).

Using the preliminary alignment, studies can be performed on the inner structure of the IKAR TPC and the new readout pad-plane. A first step is to identify the visible structures that are shown in the primary vertex xy-position shown in Fig. 7(b). The structures can be identified clearly with the photograph of the mounted readout structure. The beam spot is slightly shifted with respect to the center of the anode structure, where the single segmentation and pads are visible. Structures visible on the left-hand side are the connectors of the single pads as well as the outer rim of the downstream window. For the further analysis these structures will be excluded. In addition, the vertical wires of the grid are visible.

Based on this preliminary analysis, the alignment will be further refined. The final goal is to include the full COMPASS spectrometer information and to allow a momentum measurement of the scattered muon, which is required to reconstruct the Q^2-spectrum of elastic muon-proton scattering. With the correlations between the recoil-proton and the scattered muon in the elastic case, both measurements can be extracted and compared in terms of efficiency and resolution. Furthermore, these elastic events can be studied by considering the reconstructed beam momentum based in the BMS information. Those results can further refine the analysis methods for the final measurement and serve as input to the continuously ongoing simulation and hardware developments.

Beam Noise Influence on TPC Resolution

Compared to the Test Run in 2018, the beam size for the Pilot Run in 2021 was much more similar to the size anticipated in the final measurement, thus allowing us to study the noise induced by the beam muons inside the TPC and its influence on the energy resolution. For that purpose, several dedicated pulse generator measurements at different beam intensities were performed with the TPC filled with hydrogen at 4.3 and 7.5 bar

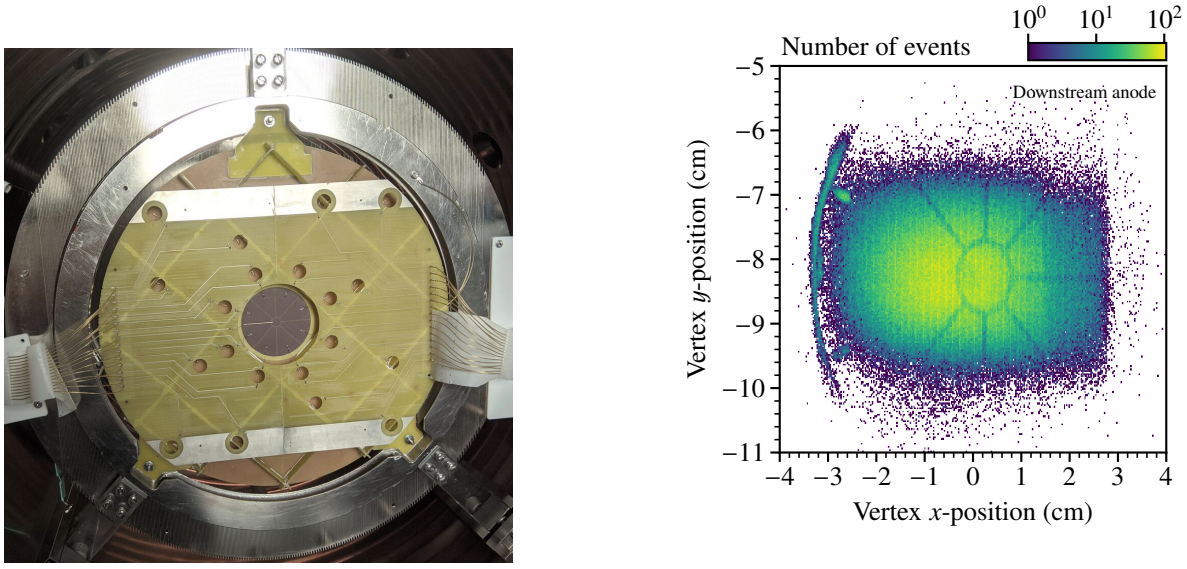

(a) (b)

Fig. 7: (a) Photograph of the mounted anode structure for the IKAR TPC, shown together with the electrical connection of the single pads and the grid; (b) Vertex xy-position at the z-position of the downstream anode shown in (b) with the single structures visible. This figure corresponds to the inner part (dark brown) shown in (a).

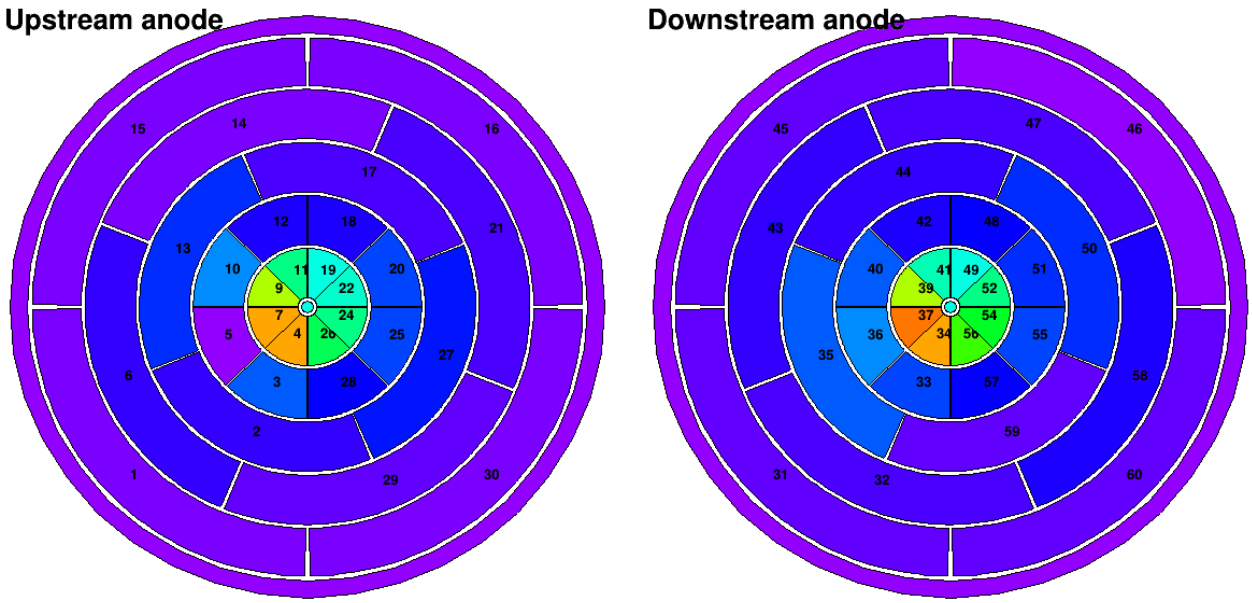

Fig. 8: In and off-spill noise difference. Warmer colors correspond to higher beam-induced noise. The single pads are numbered.

pressure. In addition, for several days the data taking was done with a helium filling of the TPC. The beam rate was monitored via the ion chamber 2 (IC2) in the beam line. The beam position can be measured using the silicon tracking detectors and controlled by the TPC itself. This can be visualized by the difference in the measured noise for the on- and off-spill regimes. The results of these studies are presented in Fig. 8. The beam spot was shifted to the left (i.e., in the Salève direction) and downwards. These findings were confirmed by the measurements with the tracking detectors.

The ionization noise induced by the beam was studied with those events, in which test pulse signals provided by a generator were sent into all channels. A series of special rate scan runs allowed to deduce a dependence of the

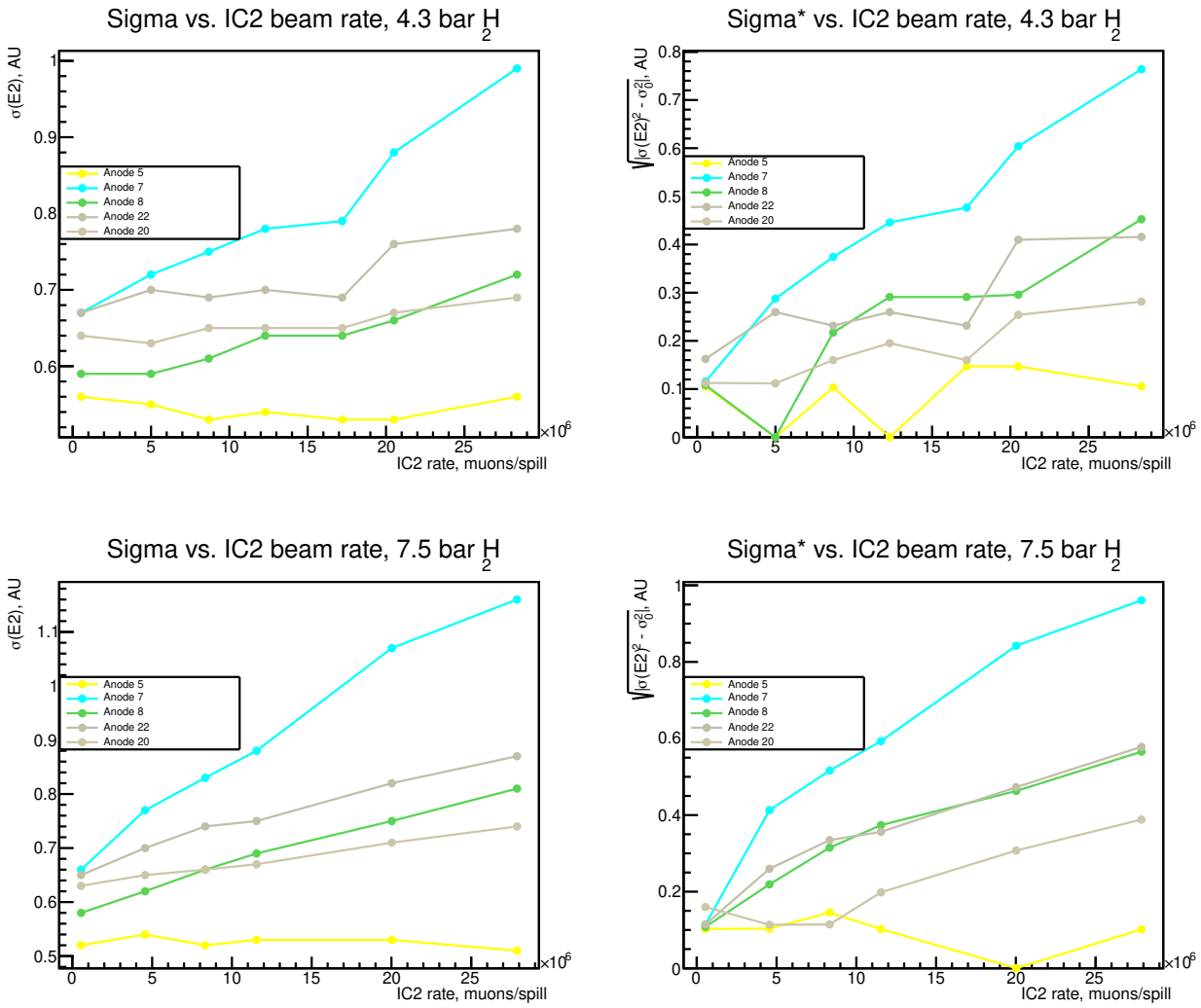

Fig. 9: Dependence of energy resolution for 4.3 bar (top row) and 7.5 bar (bottom row) on the beam intensity. Absolute (left) and no-beam corrected (right) values are shown in arbitrary units (1 AU $\approx$ 30 keV).

noise with respect to the beam intensity in a range of up to approximately 6 MHz. The preliminary results are presented in Fig. 9 and show that under the given conditions the noise remains below 40 keV even for 5.6 MHz beam rate at 7.5 bar hydrogen pressure.

Energy Spectrum on different Pads of the TPC

Signals from the TPC were reconstructed using a dedicated algorithm. The largest signal in the readout window is selected. For the discovered peak begin and end times are extracted and the signal is integrated over this range. This integral is proportional to the collected ionization charge of the recoil particle, which is deposited on the anode pad. The baseline is corrected iteratively for each event. Typical energy spectra collected for 7.5 bar pressure with the nominal beam intensity of 2 MHz are presented in Fig. 10. In general, all pads can be divided into two categories, i.e. those that are influenced by the signal of the alpha particles (from the sources placed on cathode and grid) and those that are not. Both categories contain generator signals. For the first category, the signals that are not attributed to pulses of the generator are present in both in and off-spill regime. In contrast, for pads of the second category the signals created by the recoil particle are clearly visible.

Gas Purity Control and TPC Energy Calibration

Low intensity ($\sim$3 Hz) ^{241}Am alpha sources (E_α=5.486 MeV) deposited on the cathodes of cells 1 and 2 and on the grid of cell 1 provide the opportunity to perform a basic energy calibration of the TPC and control the

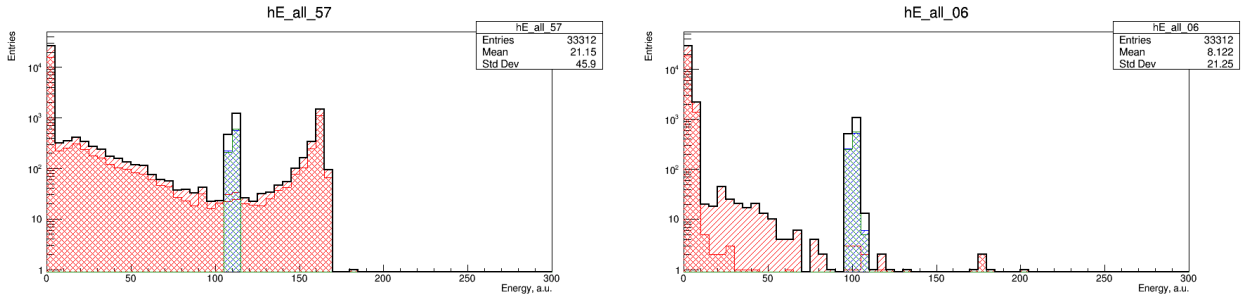

Fig. 10: Energy spectra collected during the run with the nominal beam intensity. The spectrum for pad 57 (close to the source of alpha particles) is presented in the left panel, while the spectrum for pad 6, which belongs to the second category of pads, is presented in the right panel. The blue histogram corresponds to generator signals in-spill and the green one to generator signals in the off-spill regime. The dark red histogram corresponds to non-generator signals collected off-spill while the light red one is the energy distribution for the events of the non-generator type.

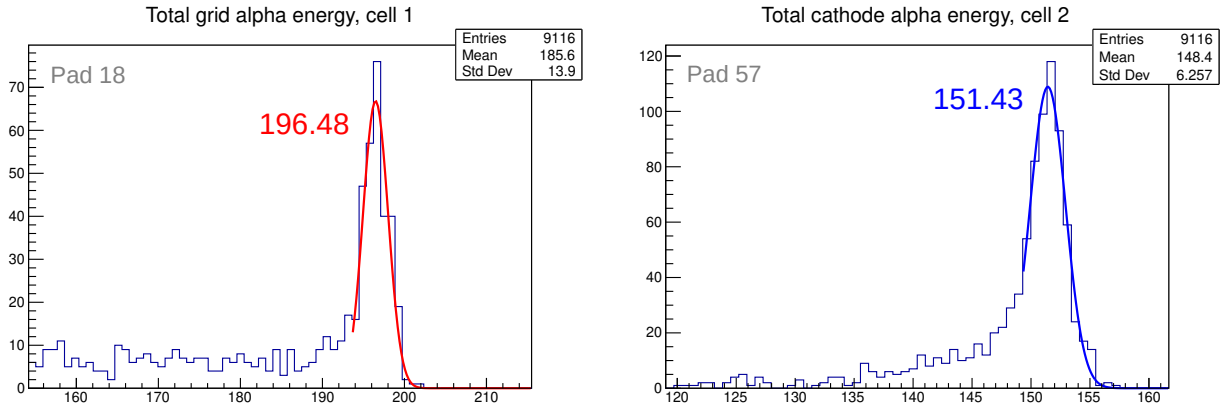

Fig. 11: Example of alpha source energy spectra for cathode and grid sources (hydrogen pressure 7.5 bar).

contamination of the gas by electronegative admixtures (such as oxygen from the air or water vapor), which reduces the total charge of the ionizing particle as it travels through the active volume. The effect of this electron attachment results in a lower energy of the signal, if the alpha source is located on the cathode and not on the grid. This data combined with precise time information providing the vertex position of the recoil proton will allow us to apply an attachment correction to the measured TPC energy in the further analysis.

The timeline plot presented in Fig. 12 indicates good purity of the gas for 4.3 bar data (first two time points) and subsequent sharp increase of attachment after the switch to 7.5 bar (remaining four time points), which occurred due to technical reasons. The last three time points show a slow improvement of the gas quality due to the operation of the gas flow system. The overall cathode alpha energy drift was 1.7% per day for 4.3 bar and 1.2% per day for 7.5 bar hydrogen pressure.

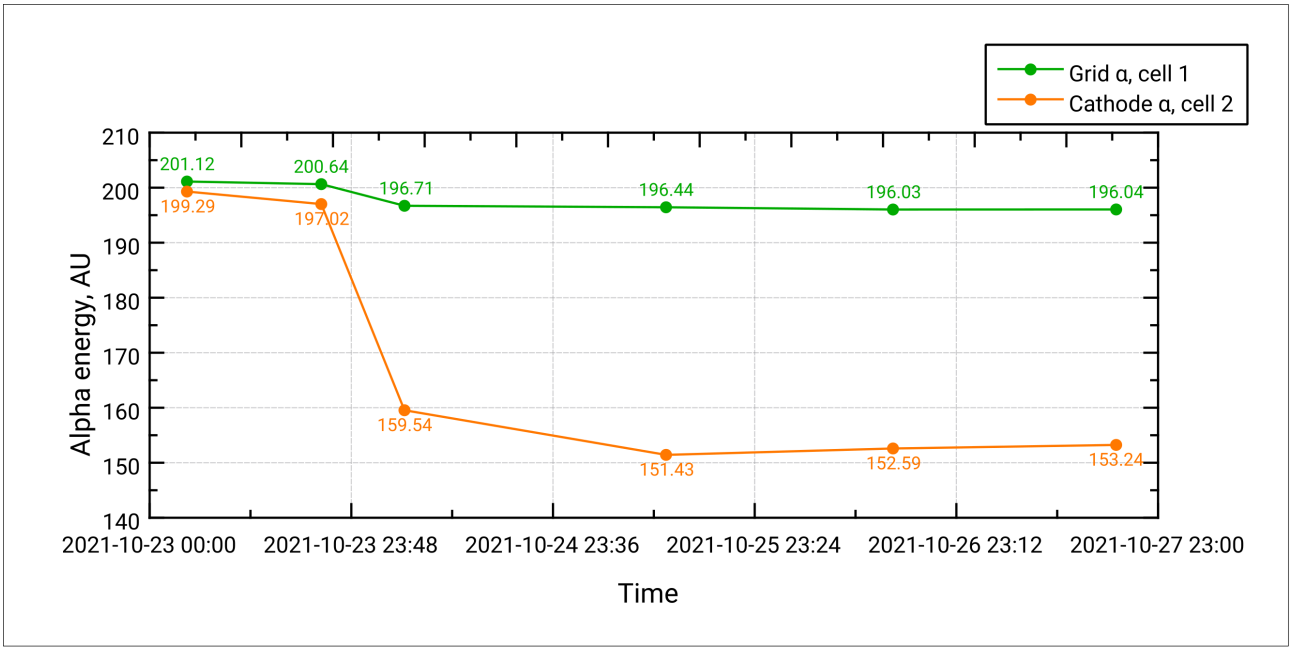

Fig. 12: Grid and cathode alpha energy evolution over time with H_2 TPC filling.

ALPIDE Beam Test Results

A beam telescope with four single ALPIDE detectors has been installed at the M2 beam line and tested during few days. A dedicated DAQ PC has been configured and installed. Muon beam with a momentum of 160 GeV/c and intensity up to 2 MHz irradiated the setup shown in Fig. 13. Readout of the detectors was based on four MOSAIC FPGA boards developed by the ALICE collaboration. All MOSAIC boards were connected to the DAQ PC via the multi-gigabit switch within the closed network. Data transfer was organized using the high-speed links (up to 1.2 Gb/s) needed for the proper operation of the AMBER tracking stations. In the current design a single plane is built up by 18 ALPIDE detectors. The detectors were read out in a free-running mode supposed to be used within the future AMBER DAQ. Valuable information related to the configuration of the detector parameters in the realistic measurement conditions has been obtained. Additional beam test with deuterons at energies 300, 800 MeV and 1 GeV has been performed at FZ Jülich in spring 2022. Similar setup as before at CERN, with single detectors readout by the MOSAIC boards, has been used. Measurements aiming cluster shape studies and rate capability were made at beam intensity from 30 kHz up to 2 MHz shown in Fig. 15. Preliminary results show no saturation of the data rate up to the intensity of 1 MHz. This test, as well as the one at CERN in 2021, is made together with the ALICE ITS collaboration. The test station with several MOSAIC boards used at CERN and later at FZ Jülich, is currently makes a basic of the R&D setup at GSI Darmstadt. Master-slave mode of the readout and effective noisy-pixel suppression are being developed.

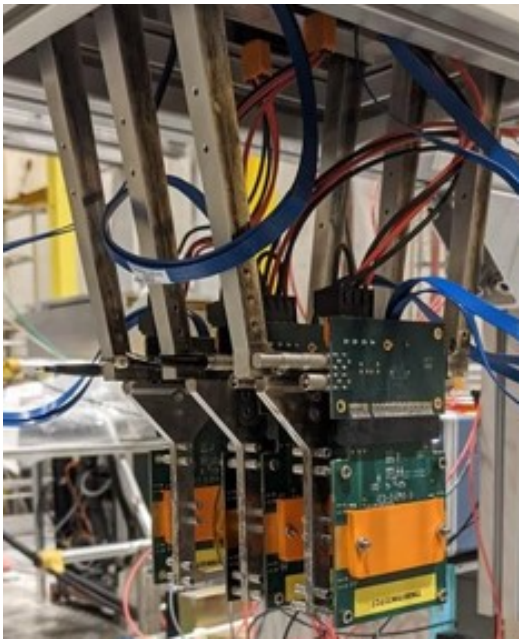

Fig. 13: ALPIDE beam telescope setup during the Pilot Run. The single chips are protected with the orange cover and the readout boards are mounted in the final holding frame of the UTS.

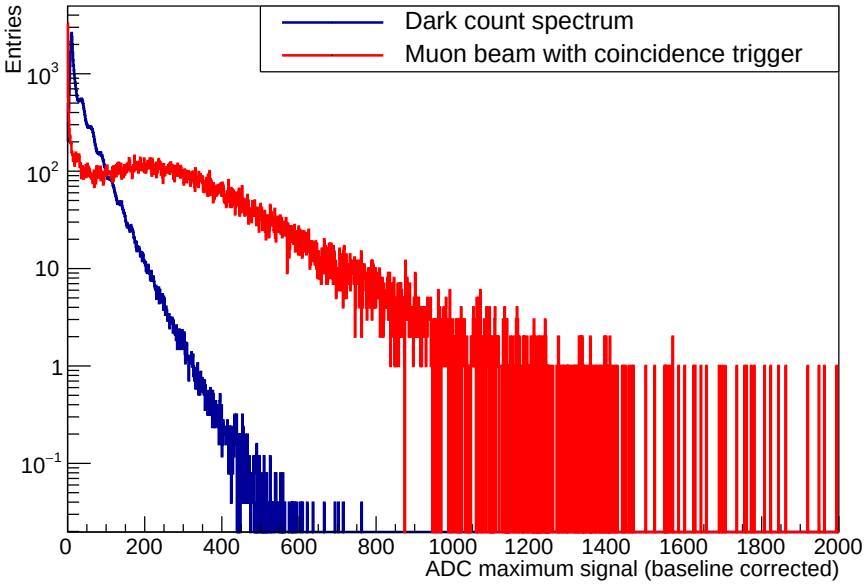

Fig. 14: Preliminary results from the SFH beam test. Comparison between the dark count spectrum (blue) and the muon beam signals (red) in baseline corrected maximum ADC channels.

2.2 Ongoing Activities and Plans for 2022

In view of a possible PRM measurement in 2023, dedicated detector tests are required in 2022 especially for the novel UTS, which combines scintillating fibers (SFH) and ALPIDE-based pixel-silicon tracking detectors (SPD). A technical drawing is shown in Fig. 16. The detectors are placed inside the UTS from the top. It will contain three planes of silicon detectors and four planes of fiber detectors. The silicon detectors will provide a precise spatial measurement of beam and scattered muon, whereas the fibers provide precise timing information for the hits in the silicon detectors. With the main design finished, detailed studies of the fiber coupling towards the readout SiPMs are ongoing. A parasitic test in the beam line during the COMPASS data taking was performed end of May 2022 to study efficiency and light yield of the fibers. Recent results from the fibers are shown in Fig. 14. The peak structure in the dark count spectrum corresponds to the number of fired SiPM cells. The measured signal has a peak at about ten photons.

The full UTS is foreseen to be tested end of 2022 in parasitic manner during COMPASS data taking. It will be placed in the COMPASS target region, where comparable beam parameters as for the proton charge-radius measurement are present. In addition, surrounding tracking detectors will allow for detailed studies of the UTS. Furthermore, it is planned to have the beam test of the UTS with the new triggerless DAQ system. More details on the UTS and the DAQ system can be found in Sec. 5.2 and Sec. 5.3, respectively. The goal is to evaluate the overall efficiency of the station as well as the association of fiber hits to silicon hits, and to identify possible challenges. The new DAQ system can be further evaluated with a focus on the the High-Level-Trigger (HLT) and the reconstruction of the new data format.

2.3 Plans for 2023

Based on current developments and time lines, a measurement of the proton charge-radius could take place in the second half of 2023 as a pilot physics run. Due to the restrictions of Russian institutes in the current situation, the development and construction of the main TPC is delayed. A finalization until next year becomes very unlikely and studies are ongoing whether the IKAR TPC could be used as fall-back solution. Limitations in the purchase of electronic components restrict the construction of new front-end electronics required for the triggerless DAQ system for a major part of the spectrometer detectors. Therefore, only first physics measurements with the PRM core setup and a reduced acceptance in the spectrometer can be performed in 2023. A minimal setup could consist of the PRM core part with TPC and surrounding UTS to determine the scattering

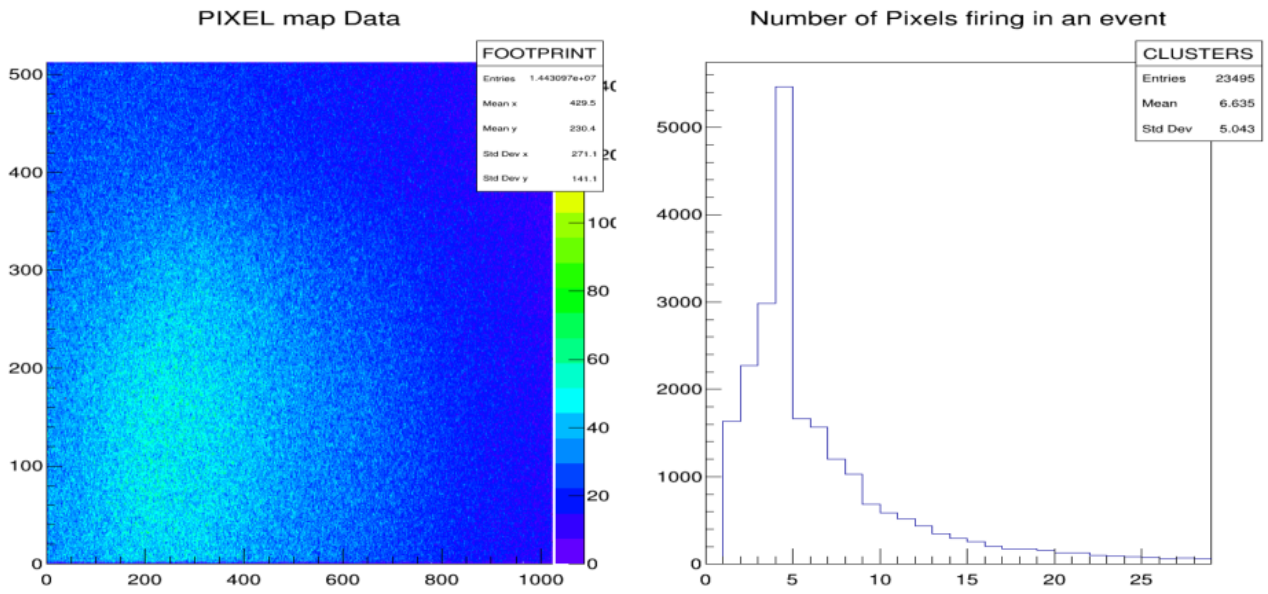

Fig. 15: Left: Beam profile measured by the ALPIDE detector. Right: Number of fired pixels per event.

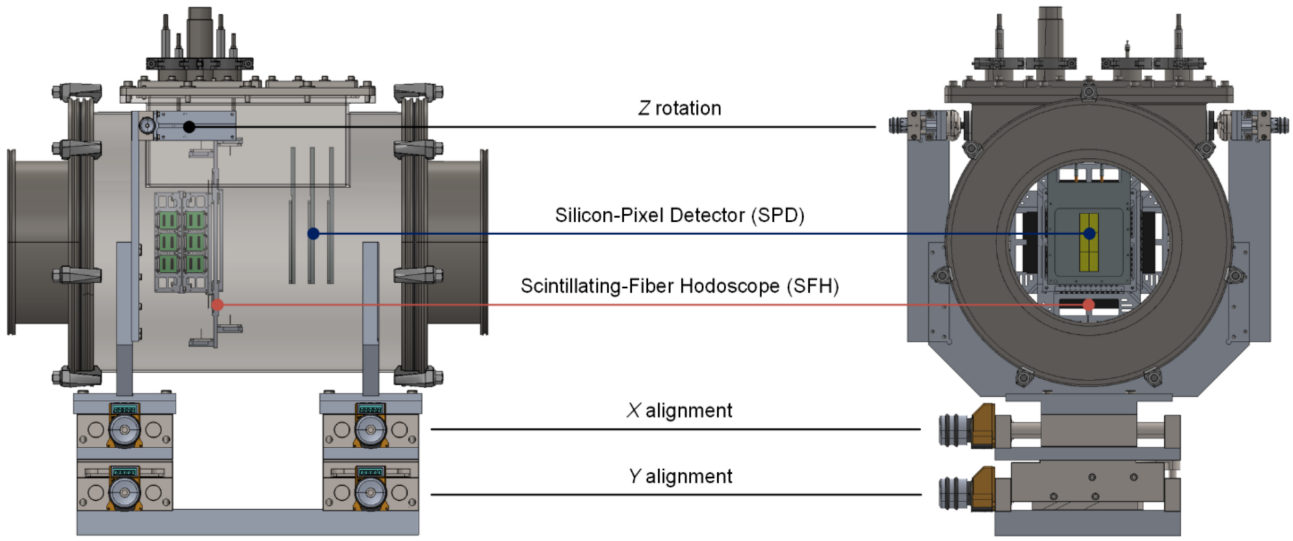

Fig. 16: Technical drawing of the UTS. The SPD and SFH detector planes are indicated as well as the positioning system.

kinematics and the BMS to measure the incoming beam momentum. As no additional detectors would be included from the spectrometer side, the momentum of the scattered particle would not be measured and muon identification could not be performed. A more extended version of the setup would be possible if sufficient frond-end electronics would become available. This would include tracking and therefore momentum measurement of the scattered muon and its identification. A preliminary study on the event reconstruction efficiency comparing vertex-only and vertex-with-momentum measurement is shown in Fig. 17. With a minimal setup, the efficiency shown in Fig. 17(a) is slightly reduced by about 0.5 % compared to the full setup. For the more extended setup shown in Fig. 17(b), the efficiency is comparable to the one with the full setup. In spite of the smaller angular acceptance of the reduced detector setup in the spectrometer, especially at larger values of $Q^2 > 0.04$ GeV$^2/c^2$, for the reconstruction of Q^2 no bias or reduction in resolution is observed.

The above described limitations will be reflected in reduced statistics and reduced Q^2 range. Although it is unlikely that a meaningful physics result can be extracted, a first evaluation of the full measurement principle can be performed. Should such a possible 75-day physics pilot run be performed with the IKAR TPC, a factor of five lower statistics has to be expected compared to the originally foreseen 150 days beam time, due to

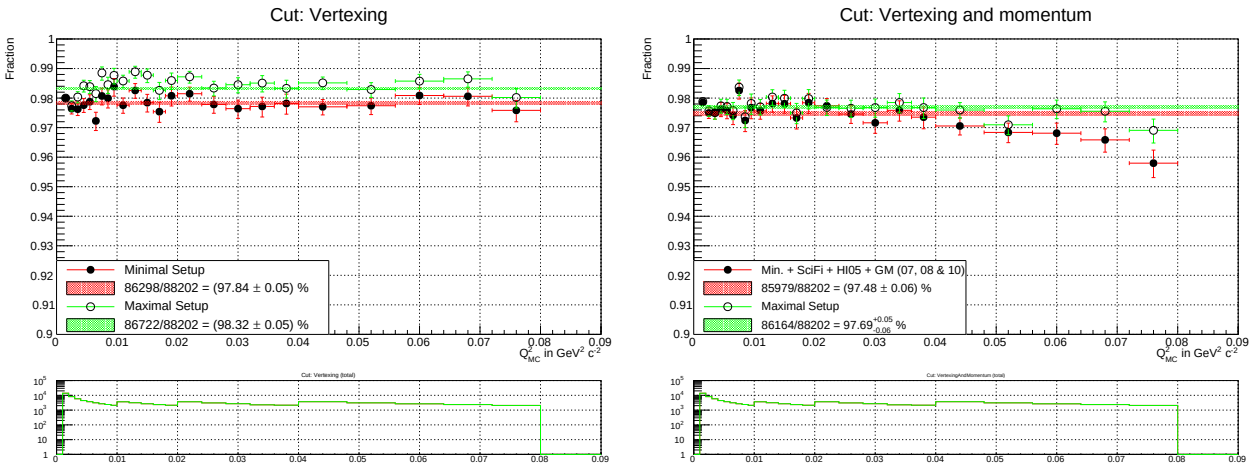

(a) (b)

Fig. 17: Event reconstruction efficiency for two possible reduced setup scenarios compared with the full setup. (a) Minimal setup with only the PRM core part and BMS. Only the incoming beam momentum is measured in this case; (b) Extended setup with detectors included in the spectrometer, which allows also a momentum measurement of the scattered muon. The bottom panel shows the event statistics in the Q^2 sub-ranges.

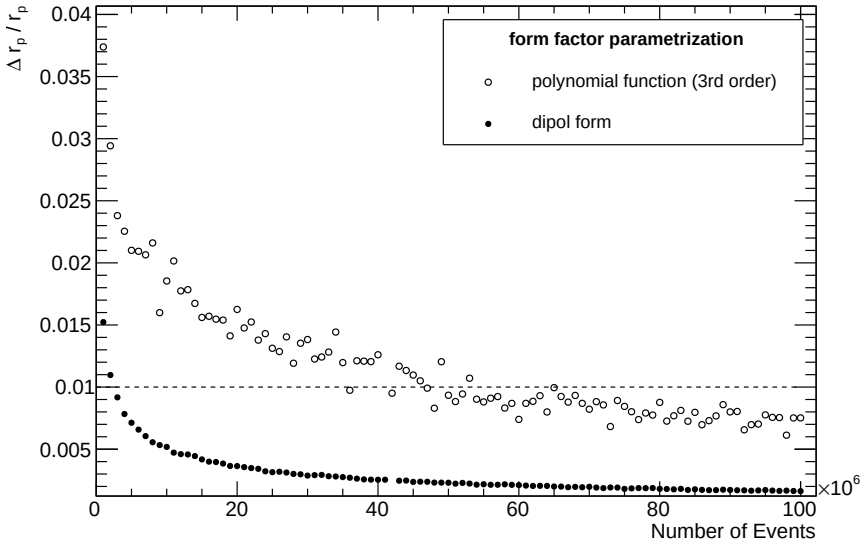

Fig. 18: Dependence of the statistical uncertainty of the measured proton charge-radius on the recorded number of events, given for two different parametrisations of the electric form factor in the initially proposed Q^2-range of $0.001 \leq Q^2/(\mathrm{GeV}^2/c^2) \leq 0.04$. The dashed line indicates the expected 1 % precision of the extracted r_p. Figure taken from [1].

the lower pressure of 8 bar instead of 20 bar and the reduced target length of two instead of four drift cells. Altogether, such a possible pilot physics-run in the second half of 2023 with about 75 days of beam time would reduce the initially envisaged number of events of 50 to 70 million down to 5 to 7 million events. In this case, the expected accuracy of below 1 % precision in the measurement will be more than a factor of two worse, which we estimate by using Fig. 18.

2.4 Perspectives for Hadron Radii Measured in Inverse Kinematics

As an extension to the Primakoff data taking with hadron beams foreseen in AMBER Phase 2, we investigate the possibility to measure hadron radii by elastic scattering off atomic electrons. This method to realize electron scattering in inverse kinematics has so far been the only access to the radii of pions and kaons, however we

currently extend the investigation to protons. This could allow for another access to the proton radius, and the method shall be valuable in terms of exploring the systematic effects of scattering experiments in the quest of measuring the proton radius. In terms of the kaon and pion radii, a measurement at AMBER will profit from the technology advancements compared the previous measurements, dating back to the 1980s [5, 6]. Detailed studies including Monte-Carlo simulations are ongoing in order to explore the potential of such measurements. The TPC volume, providing a pure hydrogen target, may serve as electron target with optimal multiple scattering conditions.

3 Anti-Proton Production Cross-Section Measurements

A dedicated measurement campaign of the the exclusive cross section $p + {}^4\text{He} \rightarrow \bar{p} + X$ is crucial for the search of Dark Matter (DM) signals in the spectra of antiprotons in cosmic rays.

The proposed experiment aims at measuring the double-differential antiproton production cross-section for different incoming proton energies (60 – 280 GeV/c) from the North Area M2 beam line, impinging on liquid-He target. The experimental determination of the antiproton production cross-section in p+^{4}He scattering is foreseen at the beginning of the 2023 run, with a preliminary test run at the end of 2022.

We present the recent developments in preparation of the measurement and the plans for the 2022 and 2023 runs.

3.1 Full MC Simulation of the Anti-Protons Experimental Setup

The layout of the COMPASS/AMBER spectrometer used for the anti-proton production measurement is based on the one used for the COMPASS SIDIS run. There are however some notable differences, in particular about the target and the detectors implementing the trigger.

A MC simulation of the anti-proton production experimental setup has been implemented in the framework of the GEANT4-based COMPASS/AMBER simulation software, called "TGEANT". This allows the complete simulation, and reconstruction, of events similar to those we are going to measure. These simulations, among other results, have been used for the optimization of the trigger detectors position, in particular of the two Beam Killers, for the study of the kinematic domain and of the spectrometer performance and as a spring board for the implementation of the M2 beam line CEDARs detectors into the simulated setup.

The experiment will be operated with a minimum-bias trigger, which includes: beam trigger and hodoscope veto, which ensures that the particle reaches the experiment within the geometrical target acceptance; beam killer 1 (BK1) and 2 (BK2), to remove the non-interacting beam particles.
In Fig. 20 and Fig. 21 the x-positions of BK1 and BK2 obtained from the MC simulation of p $+{}^4$ He events at different beam momenta are shown. The beam particles at 60 GeV/c (in blue in the figures) are very much deviated in x with respect to the nominal hadron beam momentum at 190 GeV/c. This would require a very large displacement of the BK and of the small area trackers in x, which has to be avoided. Thus a scaling of the SM1 magnet current will be necessary.

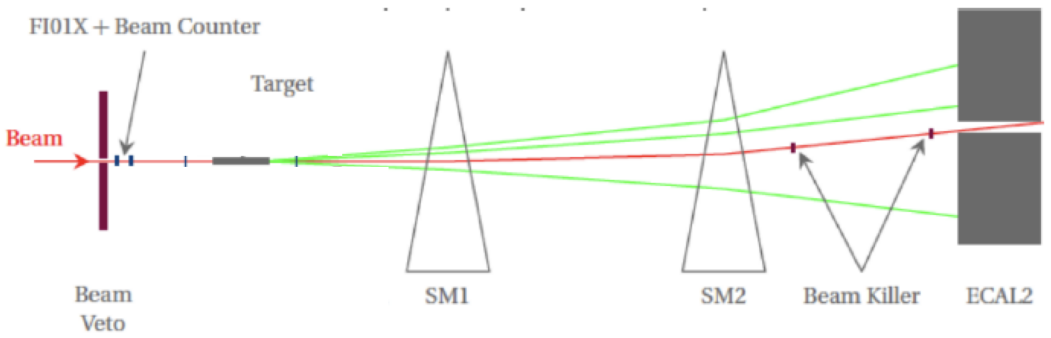

Fig. 19: Schematic view of the minimum-bias trigger setup.

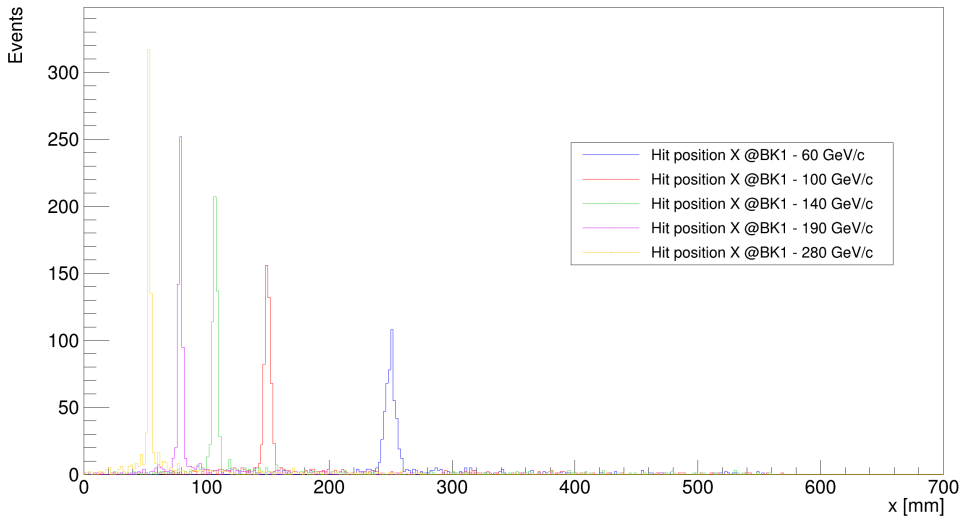

Fig. 20: Position of the beam killer 1 in the x-coordinate for different beam momenta.

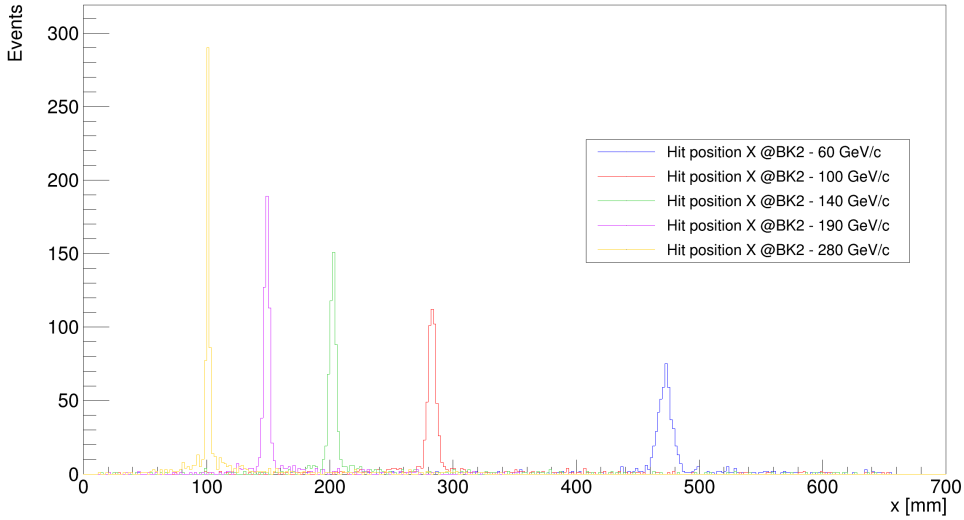

Fig. 21: Position of the beam killer 2 in the x-coordinate for different beam momenta.

The two M2 beam line CEDAR detectors are very important to identify protons in the incoming hadron beam. The CEDAR detectors are installed 30 m before the target region and they have been designed to provide fast beam particle identification at high rates for pion/kaon separation up to 300 GeV/c and proton identification down to 60 GeV/c. The two CEDARs have been object of an upgrade in 2018, including the improvement of the photomultipliers and of the read-out to withstand high-rate environments, the upgrade of the thermal system to control the stability, and the introduction of a PMT gain monitoring. In order to study the CEDARs performances with the hadron beam a simulation of the CEDARs is being implemented in the TGEANT MC of the AMBER spectrometer as shown in Fig. 22.

3.2 Study of the COMPASS RICH PID efficiency and purity

The study of the performance of the COMPASS RICH detector for antiproton identification has been continued and finalised, from the 2009 COMPASS hadron data, by the analysis of the so-called V0 decays (Λ, $\bar{\Lambda}$, K_0, $\Phi(1020)$), to determine the efficiency and purity of the RICH PID. The PID is based on an extended maximum likelihood algorithm and the cut used to identify different species relies on likelihood ratios. An optimization of these cuts was performed in particular for the antiproton PID.

In general we can achieve > 90 % efficiency in antiproton identification with some contamination at low momenta and polar angle as shown in Fig. 23.

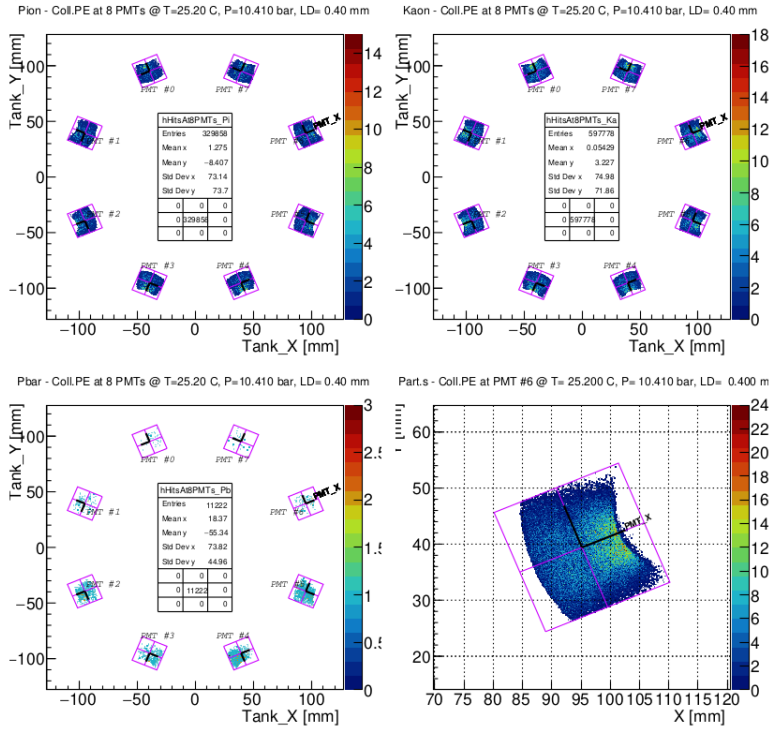

Fig. 22: Simulation of photo electrons collection inside PMTs of the CEDAR detector.

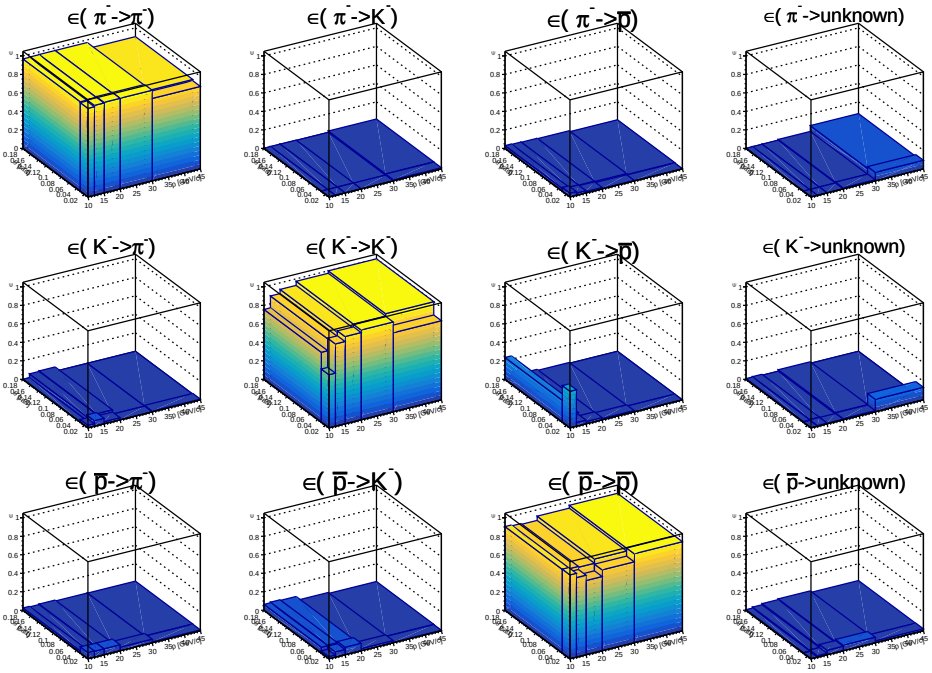

Fig. 23: Efficiency matrix for negative charged particles.

3.3 Hadron Beam Test at the M2 Beam Line

In mid-May 2020 in between NA64 and COMPASS commissioning time, 2 days have been dedicated to test the M2 beam line in hadron beam mode. In this test campaign in collaboration with the beam line experts we found good beam configurations for the energies of 60, 190 and 250 GeV/c. The beam configurations were saved to be used later in 2022 and in 2023 as base for further optimizations. Beam intensities and trigger rates were studied, the beam killers were installed and their moving platforms were tested. The position of BKs was extrapolated performing a scan of the counting rates as a function of the position along x- and y-axis. (Fig. 24).

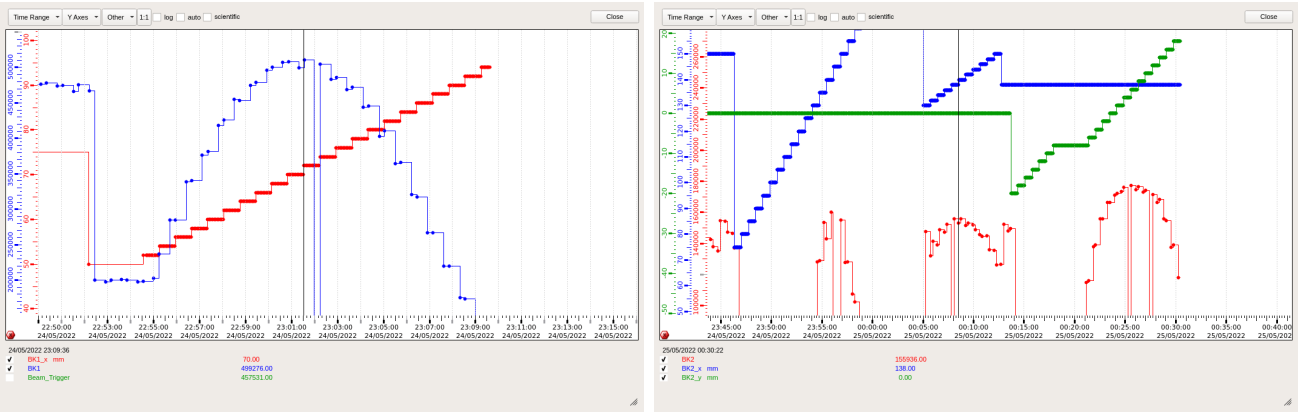

Fig. 24: Left: x-position scan for BK2; Right: $x - y$-position scan for BK2

The test was performed with the LiD target of the COMPASS SIDIS run, which is a factor 3 more dense than the liquid-He target. Nevertheless, the trigger rate was measured: a reduction factor of 80 % was achieved using the beam killers in anti-coincidence with the beam trigger.

3.4 Plans for 2022 and 2023

To perform the proposed measurement we need to go through two steps: the test run in the fall of 2022 and the data taking in the spring 2023.

The 2022 test run will be performed with the COMPASS SIDIS target, i.e. cryogenic LiD polarized. The different target introduces some limits, mostly because when compared to the liquid-He the SIDIS target is more dense by a factor 3. We will compensate the larger density by prescaling the trigger. This allows to use beam configurations similar to the 2023 data taking, with a comparable effective trigger rate.

The 2022 test runs will last for a few days, the main goal will be to collect preliminary data with the spectrometer in configuration as close as possible to the final configuration. It will be important to use beams of at least three energies, 60, 190 and 250 GeV/c. The collected data are expected to provide information about the event topologies as function of the vertex position along the 1.2 m long target. The vertex distribution along the target will need to be rescaled for the higher LiD density with respect liquid-He. Another very important topic will be the study of the RICH performance in terms of particle identification capability. At the end of the SPS proton run, we would like to load the COMPASS/AMBER target with liquid-He to test our final target configuration before the 2023 run. This test must be completed before the CERN winter shutdown, when the target cryogenic system must be warmed up before turning it off. The actual feasibility of this test within the allowed time frame must be evaluated in the fall.

In the 2023 we will start with the commissioning of the spectrometer for the anti-proton cross section measurement. This will be the first full spectrometer commissioning performed as AMBER collaboration and it will include the setup of the cryogenic system and the 1.2 m long liquid-He target. An independent commissioning will also be performed on the CEDAR detectors along the M2 beam line, although at the end the AMBER DAQ system will integrate also the CEDARs data.

Once the commissioning will be completed, we will proceed with the actual data taking at different beam energies covering at least, 60, 100, 190 and 250 GeV/c.

4 Meson structure measurement

Renewed interest in studying the structure of mesons has developed over the last decade and keeps growing, driven by its close connection to the question of the emergence of hadron mass [7–11]. In order to address this question, the AMBER collaboration has submitted in 2018 a Letter of Intent describing the full project [12]. In 2019, it was followed by a proposal for Phase-1 of the experiment [1], which was accepted in 2020. In this first phase, studying the structure of the pion will be one of the major goals of the experiment.

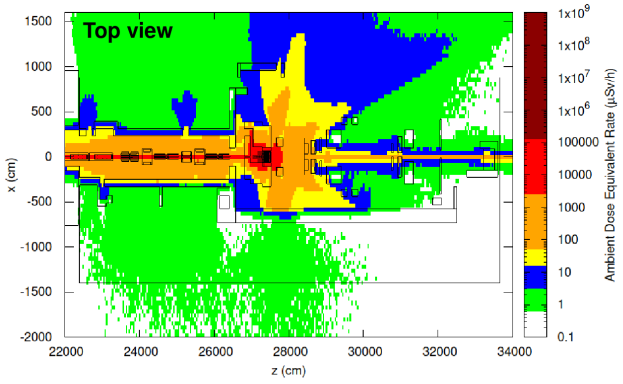

Area	Annual dose limit (year)	Ambient dose equivalent rate		Sign
		permanent occupancy	low occupancy	
Non-designated	1 mSv	0.5 µSv/h	2.5 µSv/h	
Supervised	6 mSv	3 µSv/h	15 µSv/h	
Simple Controlled	20 mSv	10 µSv/h	50 µSv/h	
Limited Stay	20 mSv	-	2 mSv/h	
High Radiation	20 mSv	-	100 mSv/h	
Prohibited	20 mSv	-	> 100 mSv/h	

Radiation Area

Controlled Area

Fig. 25: Left: Ambient dose rate from prompt radiation in EHN2. The colour scale indicates the required classification area according to the measured dose. Right: Limit of ambient dose equivalent rate for each of the radiation areas. The part of the EHN2 building that is accessible during beam time does not exceed the low occupancy supervised area classification. Taken from [16].

The golden channel to access the structure of the pion is pion-induced Drell-Yan di-muon production, as this process is theoretically well understood and can be used to extract the Parton Distribution Functions (PDFs) of the pion. However, muon pairs do not originate exclusively from Drell-Yan lepton-pair production but also from other processes, see Fig. 27. In order to interpret the data, the analysis is restricted to di-muon invariant masses between 4.3 GeV/c^2 and 8.5 GeV/c^2. As the Drell-Yan muon-pair production cross section in this range is very small, a few dozen of picobarn, a high intensity beam is required to accumulate significant statistics. Currently, the total intensity is limited by radio-protection regulations to 70 MHz with the presence of a hadron absorber and shielding right downstream of the target. In order to enhance the significance of the measurement, the containment of the radiation was studied as also improvements in track and vertex reconstruction to gain in mass resolution and to extend the region of interest to lower invariant masses.

4.1 Shielding and radio protection limitations

In order to increase the total beam intensity delivered to EHN2 while staying compliant with radio-protection regulations, studies of shielding improvement around the hadron absorber and evaluations of dose rates in the experimental area as well as in the area around the CERN domain were performed in collaboration with CERN HSE-RP and BE-EA. The Monte-Carlo description of the experimental area was combined with the one from the beam-line simulations to obtain a complete picture of radiation sources, beam losses and shielding breaches. The results were compared to those of the radiation survey campaign that was performed during the COMPASS 2018 Drell-Yan run [13, 14]. Three modifications of the shielding are proposed compared to COMPASS Drell-Yan runs. The first modification concerns the shielding breach at the junction between TT84 and EHN2, which is currently closed by a fence and to be replaced by concrete bricks. The second modification is related to the access door PPE211. In presence of CEDAR detectors, which are located in line-of-sight of the entrance door, a significant radiation dose was recorded in the building and as well as on the Heisenberg road. In order to better contain the radiation, a chicane configuration to access the tunnel area is proposed. Finally, the main modification concerns the shielding of the target area and the hadron absorber. It consists of a bunker of 2 m thick walls and 3.2 m thick roof, see Fig. 26. The detail of the modifications can be found in [15]. The prompt and residual radiation, as well as the skyshine contribution, were evaluated by HSE-RP for this configuration and for an integrated intensity of 3×10^{14} π^-/year [16]. The results were in agreement with the current radiation area classification, see Fig. 25, and would allow AMBER to run with a beam intensity about 67% higher than assumed in the proposal. The exposure of the public due to air releases in this configuration was found to be negligible. A technical note [17] is being drafted by the HSE-RP group and a joined HSE-RP and BE-EA Engineering Change Request is to be submitted in the coming months.

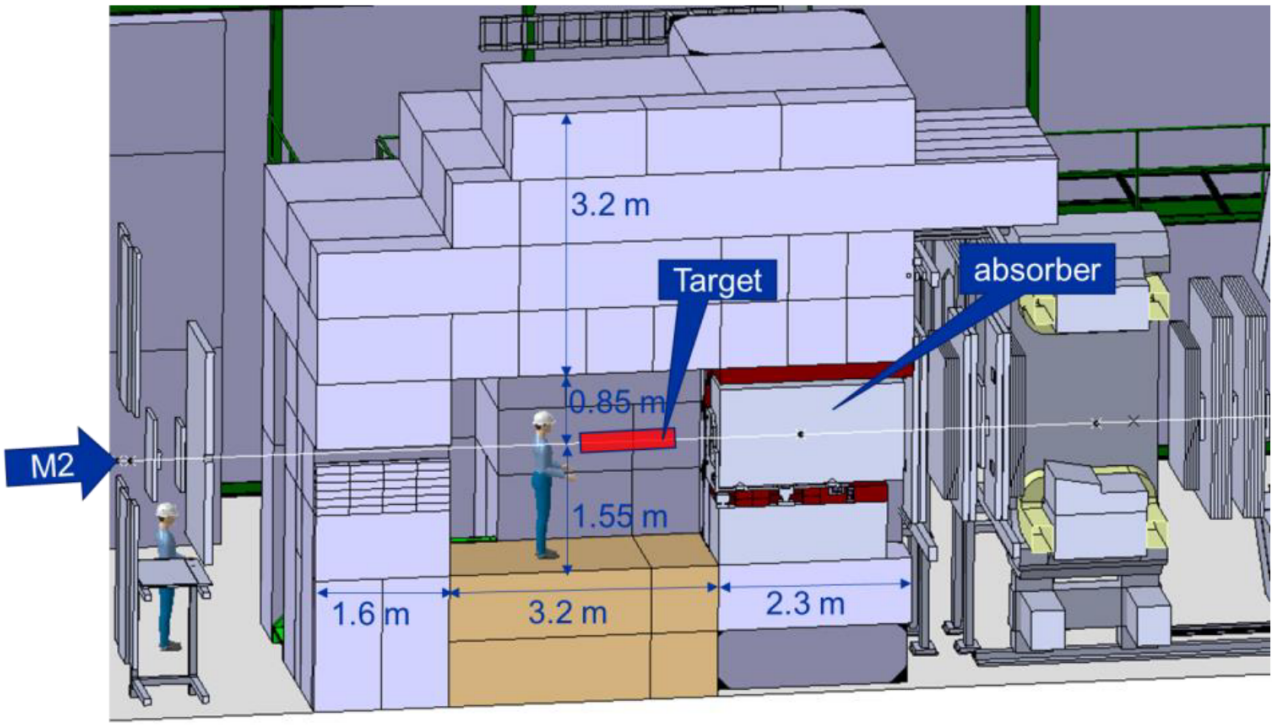

Fig. 26: Side view of the bunker design embedding the target and absorber region. Taken from [15].

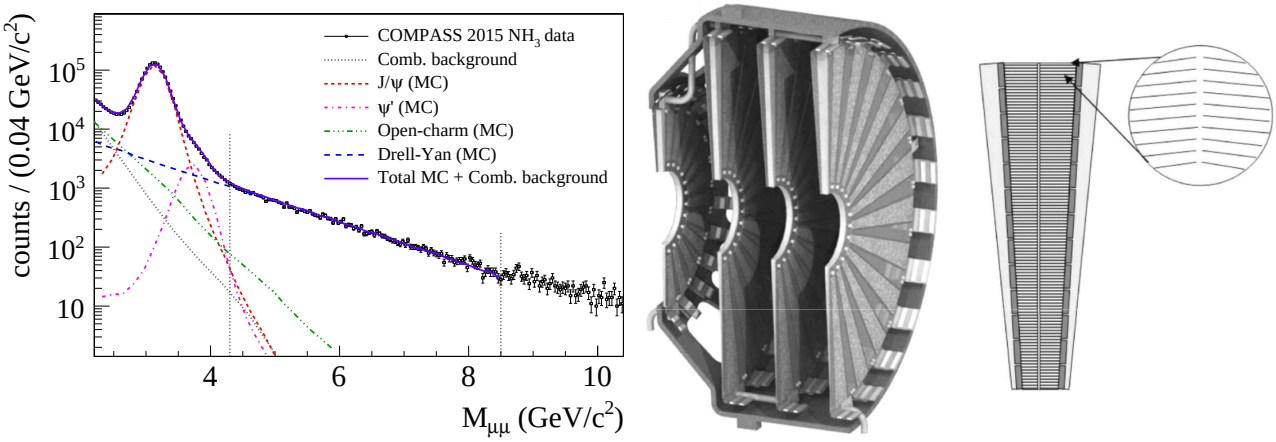

Fig. 27: Left: Di-muon invariant mass spectrum taken from [19]. Centre: Structural illustration of one endcap of the FVTX at PHENIX. Right: Wedge of the FVTX detector. A zoom of the top part of the wedge shows the two columns of silicon mini-strip as described in the text.

4.2 Track and vertex reconstruction

The accuracy of the particles' trajectory parameters determined by the spectrometer and extrapolated to the interaction point is degraded due to multiple scattering in the hadron absorber. In the proposal the benefit of a vertex detector to restore the precision of the tracking to the vertex definition and to the determination of the kinematics of the events was mentioned. Two detector technologies, scintillating fibers and silicon detectors, were under investigation. The focus is now on a silicon detector and in particular on the forward silicon vertex detector [18] (FVTX) from PHENIX. The FVTX has a shape of a disk, as shown in Fig. 27 with an external radius matching the polar angle acceptance of the spectrometer downstream of the absorber and an inner radius of 4 cm for the non-interacting beam. The detector is composed of wedges, which host two columns of mini-strip silicon sensors and readout electronics. The mini-strips are aligned in the radial direction with a pitch of 75 µm and cover an azimuthal angle of 7.5^o, see Fig. 27. Compared to the setup presented in the proposal, similar vertex resolutions and therefore mass resolutions ($\sim$ 100 MeV/c^2) are obtained with four planes of

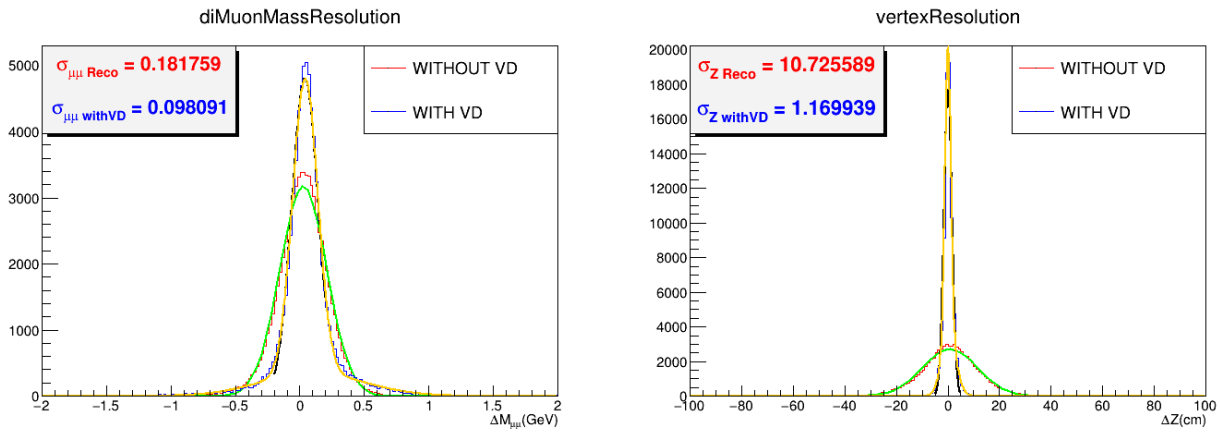

Fig. 28: Left: Di-muon mass resolution with and without the vertex detector. The yellow (green) line corresponds to a fit by a Gaussian of the distribution with (without) the vertex detector. Right: Same as on the left for the vertex resolution.

detectors instead of twenty, see Fig. 28. This reduction of number of tracking planes allows also the targets to be placed closer to the spectrometer, which is more favourable from the acceptance point of view. Optimisation of the track and vertex reconstruction algorithm as well as a more detailed description of the FVTX in Monte-Carlo simulations are still ongoing but an increase of 35% in statistics seems achievable from the extension of analysis mass range and acceptance.

4.3 Possibility for kaon structure studies

Precise measurements dedicated to the study of the structure of the kaon [12] were initially foreseen for a second phase of the AMBER experiment, using a high-intensity kaon beam produced using the radio-frequency separation technique [20]. However, the recent study from the CERN beam department seems to indicate that the intensities attainable by this technique will not meet the requirements for high statistics kaon-induced Drell-Yan measurements [21, 22]. Considering the great interest for the structure of the kaon and the poor statistics provided by the up to now only experiment more than 40 years ago [23], it seems judicious to evaluate the possibility of satisfying the demand using the M2 conventional beam. Exploiting the $\sim 2\%$ kaon component of the hadron beams (positive as well as negative), parallel measurements to the ones on the pion can be envisaged. Assuming the same conditions as described in the proposal, *i.e.* 213 days of positive hadron beam and 67 days of negative hadron beam, with an intensity of 7×10^7 particles per second and an average of 3,800 spills per day, a more precise measurement of the valence u-quark component in the kaon relative to the one in the pion can be obtained with the same experimental setup. In addition, a first evaluation of the sharing of the momentum fractions in the kaon carried by sea quarks and by the valence u-quark can be performed. The projected statistical uncertainties for the two observables are shown in Fig. 29. Including the possibility to release the limit on the maximum intensity due to radio-protection, the statistical uncertainties shown in Fig. 29 would be reduced by factor of $\sim \sqrt{2}$, so that the AMBER measurements would increase the world data set statistics on negative kaons by a factor of ~ 6.

However, excellent beam particle identification is even more crucial for kaon measurements than for pion measurements. Given the more abundant pionic component of the beam, a small percentage of kaon mis-identification would not affect the results significantly and can be included in the systematic. On the contrary, even a small amount of mis-identification of pions in the hadron beam as kaons can severely affect the results. The discrimination of pions from kaons can be ensured by majority discrimination (signal in coincidence from 6, 7 or 8 out of 8 PMTs) provided by the CEDAR-N detectors for a small-divergence beam. At 190 GeV/c beam energy, the beam divergence must not exceed 60 µrad for efficient tagging. At the CEDAR location of the M2 beamline, the divergence of the beam is presently about 130 µrad (squared sum of transverse directions), which is incompatible with this approach. Instead, the trajectory information of the particles reconstructed by the beam telescope can be used to predict the location of the PMTs that should have fired based on the particle ID. This method was developed and used successfully by the COMPASS experiment [25]. An efficiency of $\sim$87%

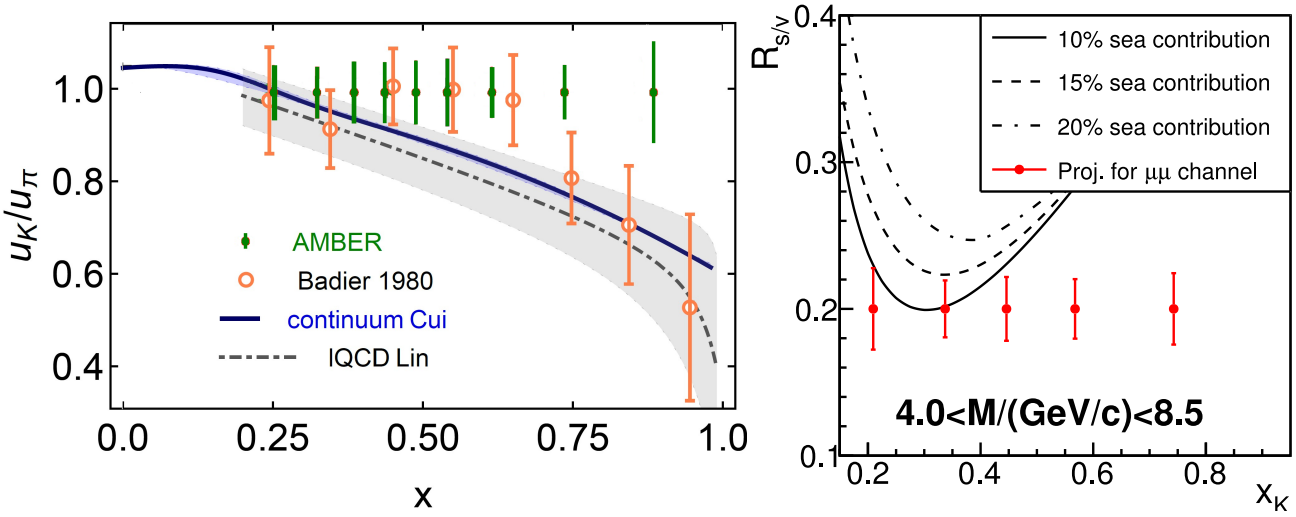

Fig. 29: Left: Projected statistical uncertainties on the kaon-to-pion Drell-Yan yield ratio with M2 conventional beams for the mass range $4.0 < M_{\mu\mu}/(\mathrm{GeV}/c^2) < 8.5$ in green, compared to the measurements from NA3[23] in orange, prediction using continuum methods[9] in blue and lattice-regularised QCD calculation[24] in black. Right: Projected statistical uncertainties on the ratio of the K^+-induced Drell-Yan cross section on carbon to the difference of K^--induced and K^+-induced ones and compared to different kaon momentum fractions carried by sea quarks derived from SMRS pion PDFs by interchanging d-quarks with s-quarks.

was achieved with a level of impurity of about 3.2% for the 2008 data taking with a hadron beam intensity of 5 MHz (at least a factor 14 lower than considered for Drell-Yan measurements).

In order to improve and guarantee successful particle identification at high intensities, two aspects should be addressed: the accuracy of the beam trajectory parameters, and the minimisation of the divergence of the beam at the CEDAR location. For the former, additional tracking detectors are envisaged and will be validated with Monte-Carlo simulations. The beam line description provided by CERN BE-EA was integrated into the AMBER simulation chain, while the integration of CEDAR detector is still ongoing. The simulations will be first compared to COMPASS 2018 Drell-Yan data for validation and then used to optimise the AMBER beam telescope. Concerning the reduction of the beam divergence at the CEDAR location, first studies were performed by the CERN BE-EA group [26]. The main results are shown in Fig. 30. In the current configuration, only 23% of the beam falls within the limits of particle identification based on majority discrimination. Currently there are segments of the beam line in the air, which add up in total to a length of 80 m. Integrating those segments in vacuum would reduce the divergence by about 8% but increase the transmission by 20% (thanks to a more efficient collimation scheme in this condition). In order to further reduce the divergence of the beam, a new collimator was simulated at about 300 m downstream the production target and the beam optics was tuned to enlarge the size of the beam at the CEDAR location, which according to Liouville's theorem implies a more parallel beam. In such a configuration, about 70% of the beam would be identified with majority signal in the CEDARs. The results are promising, the studies should be pursued and analysed carefully.

4.4 Plans for 2023

As the beam particle identification is crucial for a successful program to improve the world data on the structure of the kaon, the possibility to perform dedicated tests with CEDAR detectors at high intensity with the beam telescope from the AMBER anti-proton production setup is being discussed with CERN HSE-RP. The data would provide valuable information, which can be used to validate the Monte-Carlo simulations.

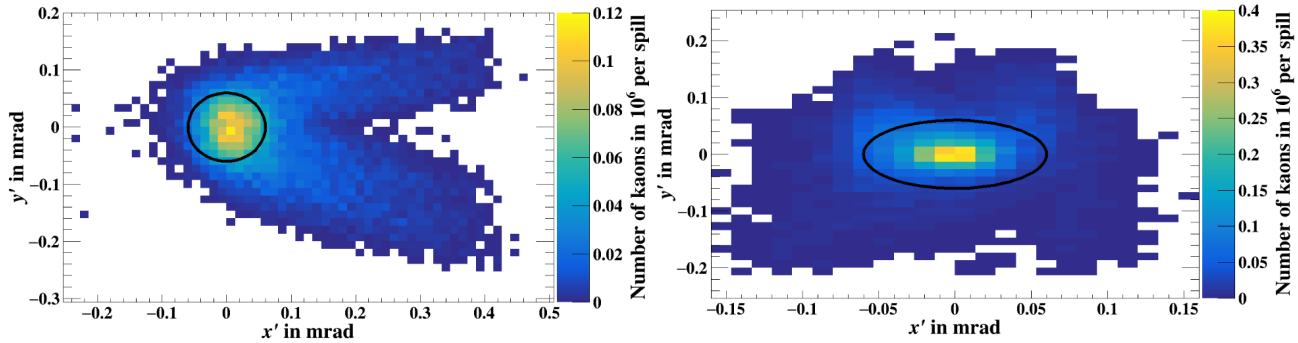

Fig. 30: Left: Divergence of the beam in horizontal and vertical direction at the CEDAR location in the current beam line configuration. The black circle represents the limit of 60 μrad for particle identification with majority signal, which contains 23% of the beam. Right: Same as on the left with beam line in vacuum and with an additional collimator located about 300 m downstream the production target and new optics tuning. In this configuration, 70% of the beam has a divergence smaller than 60 μrad.

5 Hardware

5.1 TPC and Gas System

In Fig. 31 the technical drawing of the main TPC is shown. Recently, a significant amount of parts of the inner structure for the new main TPC have been manufactured. These are a half of required number of high-precision rings, which are necessary to produce uniform electric field inside the TPC cell, prototypes of anode plane, grid PCB and corresponding support rings, and other elements required for the assembling. A test assembly has been started (see right panel of Fig. 33).

The TPC is operated in charge-collection mode with no amplification requiring to achieve and maintain for long operational time oxygen and water contamination below the 100 ppb level. This is critical for the constant energy calibration with respect to the recoil position in the TPC cell (see studies presented in Sec. 2.1.2). This goal can be achieved *via* the use of a dedicated gas re-circulation system with specific filters which absorb water and oxygen contaminants entering the TPC volume. It consists of tree main elements: a high-purity pump, a Zeolite-based filter and two mass flow-meters. The system is being engineered and built for its commissioning in 2023. The scheme is illustrated in Fig. 32.

The TPC pressure can be adjusted via the two mass-flow controllers MCF1 and MCF2 installed at the input and at the output of the TPC volume. This solution guarantees a pressure stability $\Delta P/P \approx 10^{-4}$. The automatic adjustment of the two flow controllers allows to operate the TPC in the whole pressure range between 0 and 20 bar. The gas flow can be regulated from 0 to 30 Nl/m. Due to the high purity requirements and the need to circulate hydrogen, helium and nitrogen a membrane-based pump is the adopted pump technology. The pressure modulations induced by the pump membrane will be dumped via a dedicated system of expansion volumes. A non-commercial Zeolite-based filter operated at liquid nitrogen temperature will be employed to capture water and oxygen impurities whose values will be continuously monitored via a set of dedicated sensors. The sketch of the purification unit is presented in Fig. 33. The purification unit consists of three volumes. The inner one contains Zeolite to adsorb admixtures. It is surrounded by the liquid nitrogen volume. The outer vacuum volume will provide a thermal stability of the system. The technical drawings of the purification unit are prepared and a production of the first prototype has been started in May 2022.

A PLC-based system, the expanded and upgraded version of the one used for the pilot run, will be deployed. It will act as supervisory manager of the TPC and gas system operations, it will be finally integral part of the experiment safety chain.

5.2 Unified Tracking Station

The scattered muon trajectories and the muon scattering angle is measured by the target tracking system consisting out of four UTS. This system consists of Silicon-Pixel Detectors (SPD) based on the ALPIDE monolithic

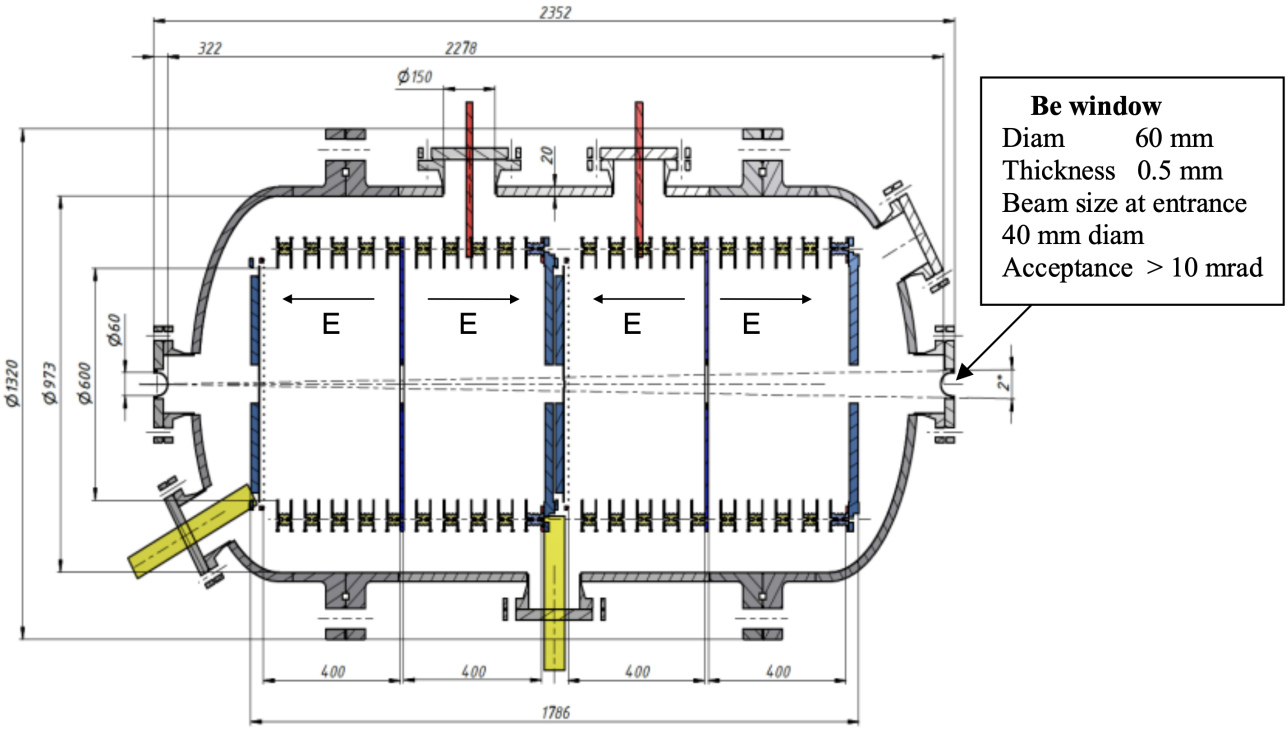

Fig. 31: Technical drawing of the main TPC. Dimensions and drift fields are indicated as well as the properties of the beam windows.

active pixel sensors (MAPS) and Scintillating-Fiber Hodoscopes (SFH) as shown in Fig. 16. The SPD cover a cross-sectional area of 9x9 cm^2 providing excellent spatial resolution of about 8 µm but require an integration time of about 5 µs, which results in pile-up hits in these detectors. Complementary, the SFH have a superior time resolution of about 300 ps and thus provide a precise timing information for each reconstructed trajectory to disentangle pile-up hits in the SPD. An active area of 9.6x9.6 cm^2 ensures a full coverage of the SPD. The time and space resolutions of the SFH are sufficient to provide a unique hit-time association between the SFH and SPD for beam intensity even ten times higher than the one presently foreseen for the proton-radius measurement. The results of studies on different fiber sizes at various beam rates are shown in Fig. 34. Even with a simple association method an efficiency of 99.8 % can be achieved at the expected beam rate of 2 MHz for the proton-radius measurement with 500 µm fibers. The SFH is a novel technological development required to achieve the beam rate capability of the AMBER tracking system based on the ALPIDE MAPS. Each station consists out of three layers of silicon planes and two planes of scintillating fibers. A total of four stations enclosing the TPC target region is required for a precise tracking of the muon trajectory.

5.2.1 Scintillating Fiber Hodoscope

ng its y-axis (the z-axis is pointing in beam direction) to provide a coarse spatial resolution. To increase the detection efficiency and to enhance the effective pitch of the detector, we use two adjacent layers of fibers for each orientation, shifted by 250 µm relative to each other; this results in an equivalent pixel size of 250 µm and an active area of 9.6x9.6 cm^2. The fibers will have a length of about 40 cm and their scintillation light is detected via commercially available 64-channel arrays of silicon photomultipliers (SiPMs). Each fiber is read out by one SiPM at each end, in order to suppress the dark counts rate of the sensors by requiring coincident signals from both sides. The SiPM signals are digitized by the Citiroc [27] application-specific integrated circuits (ASICs) specifically designed for the readout of photo detectors with intrinsic amplification, and digitized by dedicated time-to-digital converters (iFTDC). The overall system minimizes the amount of material crossed by muons in terms of radiation length, and thus minimizes multiple scattering affecting the measurement at small scattering angles and therefore low-Q^2 values. The design of the new SFH builds on our experience gained in the development of other scintillator detectors using the same type of fibers, albeit with a larger cross-section of 2 mm [28, 29]. This combination of thicker fibers and SiPM was characterized and evaluated in several test

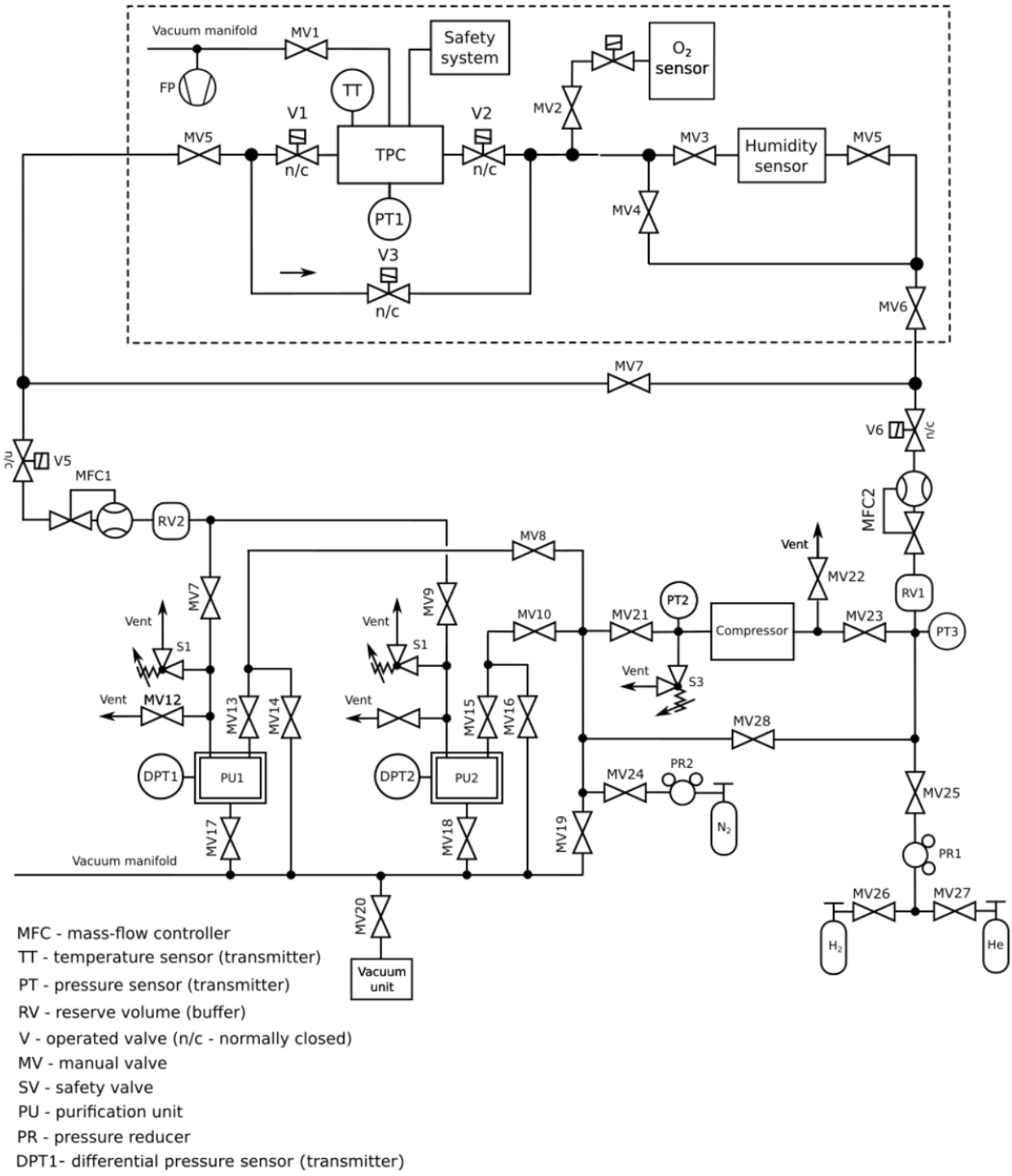

Fig. 32: Schematic of the main TPC gas system. The main components are illustrated.

experiments at the Paul-Scherrer Institute (PSI). The data allow validation of the GEANT4 based simulations. For the fibers envisaged here, minimally ionizing particles generate about 825 photons in a single fiber, of which about 50 to 75 reach a SiPM at each end of a straight fiber. Taking into account the photodetection efficiency of the SiPM, 100 GeV muons generate on average 30 photoelectrons, with a most likely value of 25 photoelectrons. Due to geometric constraints, some fibers must be curved; for these, we expect an average of 15 photoelectrons. With each layer containing 192 fibers, i.e. 768 fibers per SFH station, for four SFH stations 3072 fibers and 6144 SiPM are required. For first detector tests, a partially equipped SFH will be built with a total of 768 readout channels. This will also allow us to test optical cross talk.

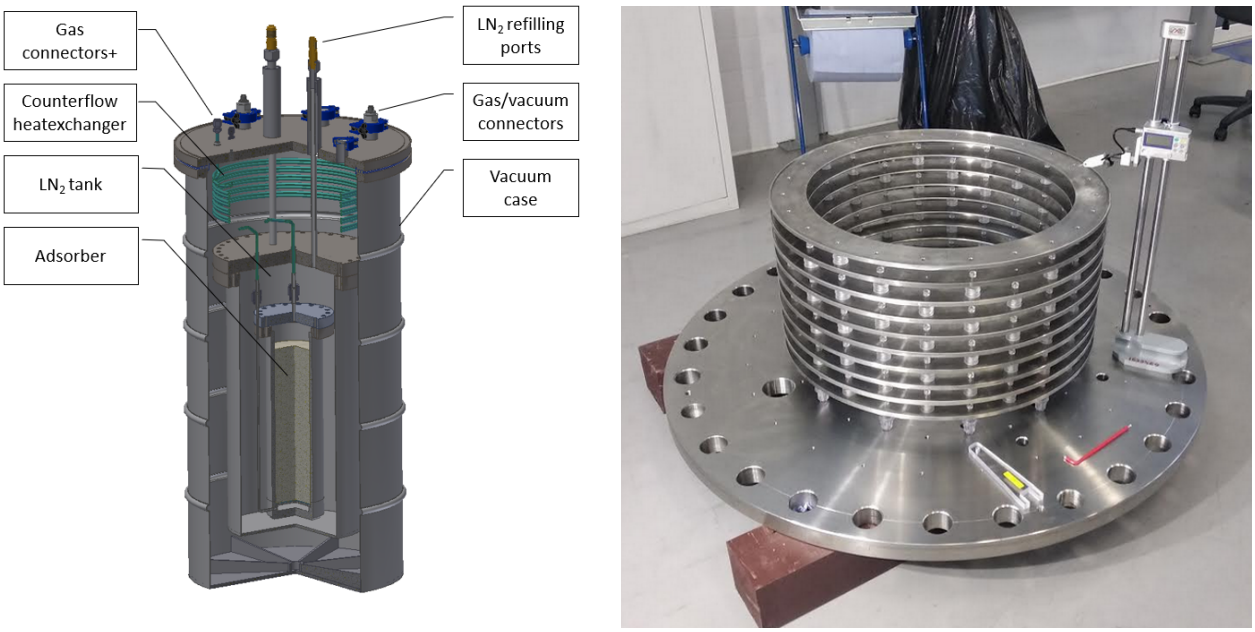

Fig. 33: Left panel: sketch of the Zeolite-based purification unit. Right panel: sample of preliminary assembling of the inner structure.

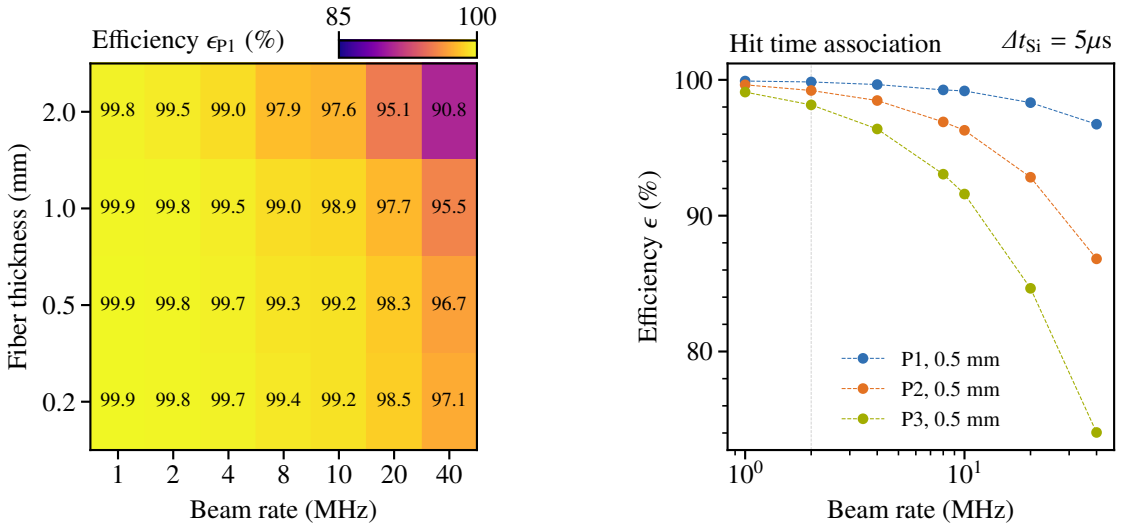

(a) (b)

Fig. 34: Simulation results on a simple hit association algorithm efficiency at various beam rates for different fiber thickness for the SFH (a) and at the three planes of the SPD for 500 µm fibers (b).

5.2.2 Silicon Pixel Detector

The Silicon Pixel Detector part of the UTS is designed to provide a high-resolution measurement of the tacks. To achieve that goal, we are qualifying the ALPIDE ([30]) sensors as the base of the Silicon Pixel Detector. This sensor can provide an excellent spacial resolution for the hits relying on 28x29 µm^2 pixels and providing a $\sim$ 5 µm resolution for single clusters. To instrument the 80x80 mm^2 surface that would be compatible with the SFH active area and the TPC entrance window acceptance we are expecting to use 18 30x15 mm^2 ALPIDE sensors per plane arranged in an 6x3 array. In total 3 planes per UTS are planned. Each plane will need a complete infrastructure comprising a support frame, integrated cooling and the readout of the ALPIDE sensors. The support frame is made of aluminum in a way to provide the gas tightness of the UTS volume and to avoid any metal elements in the active acceptance Fig. 13. The cooling system needs not only to dissipate the produced 50 mW/cm^2 power but also to reduce the material budget in the active acceptance and provide

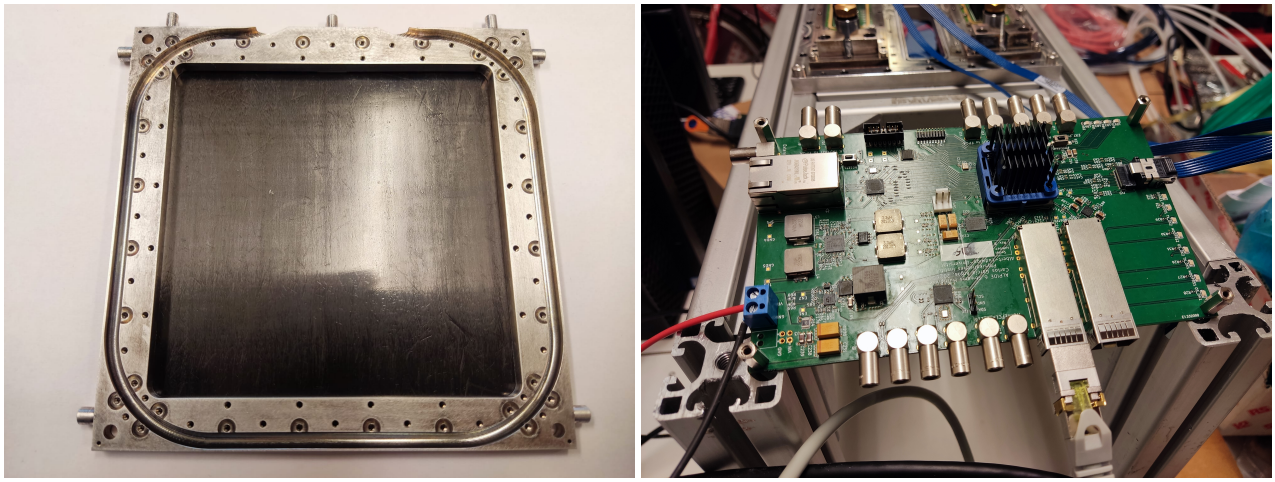

(a) (b)

Fig. 35: In (a) the thermoconductive carbon fibre plate with the holding frame is shown. (b) shows the FPGA prototype.

the support for the ALPIDE sensors. To that goal, the ALPIDE sensors are expected to be mounted on a thermoconductive carbon fibre plate (Fig. 35(a)) that would allow to place them on beam with a reduced total material budget per plane of $\sim 0.3\ X_0$ and would conduct the generated heat to the periphery where it will be removed by the water coolant circulating in copper pipes. Presently we have designed and produced a first prototype of the support and of the cooling system. We are currently carrying out the qualification of the support and of the cooling system with the goal of confirming the design choices and the previously done simulations on a real hardware. Moreover, the main task of qualifying the ALPIDE sensor for the continuous mode operation in a 2 MHz beam environment is ongoing. Lately we have tested a MOSAIC based ([31]) R/O chain compatible with the continuous readout obtaining a first data sample from a test beam at Jülich (Fig. 15). The data is being analysed and we are preparing to continue the test campaign in the next months with more ALPIDE sensors. In parallel to the "on UTS" part of the Silicon Pixel Detector a big effort is conducted for the preparation of the DAQ modules that would fulfil the task of ALPIDEs control and their data flux synchronisation and integration into the data flux of the new iFDAQ AMBER trigger-less acquisition system ([32]). Those modules are based around an FPGA and the prototypes have been already produced, the Firmware is being designed (Fig. 35(b)). We plan to have a test of this new readout modules later this year together with the Silicon Pixel Detector test.

5.3 DAQ

A novel architecture of streaming read out was selected for the data acquisition system. Developments started already in 2018. This type of acquisition allows to combine information of very slow detectors such as the TPC, where the drift time is about 100 µs, with fast detectors, such as the SPD and SFH, which have time resolution of 5 µs and 300 ps respectively. The front-end electronics processes all signals and marks them with timestamps. For some detectors, such as the ECAL, a complex signal analysis is performed on the front-end board in order to extract signal amplitude and timing. According to the timestamp information, data are merged in time slices of 1-2 ms length. The time slices are perfectly synchronous for all detector types, they contain the complete data for this time period, which is used for the so-called time slice building. Internally, the time slices are divided into images. The image length can be individual for each detector type and it is multiple of the time resolution of this detector. The time slice building is performed by an FPGA card, and the data are distributed on up to eight online computers. From there, they are transferred to local disk storage. The system will be capable to process about 5 GB/s, resulting in up to 9 PB during a data taking period. The data are then analyzed and reduced in the high-level trigger (HLT) computer farm using different event selection algorithms. Those include a kink reconstruction based on the information from the target tracking stations, in combination with information of the recoil proton detected in the TPC. The reduced data set is stored at the CERN Tape Archive (CTA).

In 2021, we started to build the DAQ infrastructure for the PRM measurement. We installed fibers between the

583 experimental area and DAQ room, part of which were used for the pilot run already. We installed and tested
584 a new network based on a high performance Ethernet switch. The switch provides high bandwidth interfaces
585 between readout computers and HLT nodes.
586 Using existing hardware and computing resources we successfully performed the following DAQ tests:

587 – the design performance of 1 GB/s for a single readout computer together with 250 TB local disk storage
588 was achieved;

589 – a performance of a single HLT compute node was varied between 300 and 800 MB/s depending on
590 complexity of event selection algorithms;

591 – the time slice builder was tested at full speed using FPGA-based data generators instead of FE electronics.
592 A data rate of 5 GB/s was achieved, exceeding the expected data rate during the PRM run of 1-1.5 GB/s.

593 The final PRM DAQ will consists of four readout computers and up to eight HLT nodes operated in parallel.

594 A so-called iFTDC system was developed by the collaboration for the COMPASS experiment and consists of
595 a 64-channel FPGA-based readout system with a time resolution of 150 ps. This iFTDC was already tested in
596 streaming mode together with COMPASS MWPC detectors and demonstrated the expected performance. This
597 system will be used for instance for the SiPM-based SFH readout.

598 Althought we consider different algorithms for the PRM run data reduction, the primary option for HLT is the
599 TPC's recoil proton trigger. The experience of the performed test and pilot run described in Sec. 2.1 suggests
600 that we can reduce amount of data by about two order of magnitude down to 20-30 MB/s. Studies are ongoing
601 for further evaluation.

602 6 Publications, presentations to conferences and collaboration matters

603 Over the last year, the AMBER Collaboration has started to formulate a procedure for its publication and pre-
604 sentation activity. The Publication Committee (PubCom) was created with the mandate to

605 – coordinate and monitor the internal approval process of all AMBER publications;

606 – solicit, distribute and allocate talks and presentations through the collaboration.

607 The main goal of the PubCom is to ensure that AMBER maintains the highest possible standards for results
608 of any type that are released publicly, whether they are oral presentations or posters, conference proceedings,
609 release of electronic archives, or journal articles. The AMBER PubCom nominally has four members who serve
610 two-year terms. Its members are chosen to cover the entire scientific program of the collaboration, including
611 the second phase of the experiment.

612 In its initial phase, the PubCom is focusing its attention on conference contributions, which are done on be-
613 half of AMBER Collaboration, since no new scientific results are available yet. The PubCom provides a single
614 contact point for conference organizers with AMBER to ensure that AMBER is visible in the physics com-
615 munity through a prominent presence in relevant conferences, workshops and schools. The list of upcoming
616 conferences is maintained by the PubCom and is advertised within collaboration on a regular basis. The Pub-
617 Com maintains transparency in order to ensure that presentations are shared in a fair manner among AMBER
618 collaborators, and provides editorial help with proceedings made on behalf of AMBER.

619 A set of rules and guidelines has been formulated to ensure a consistent and high quality in the contributions
620 made on behalf of AMBER. Adherence is verified through rehearsals within the collaboration. Those rehearsals
621 are intended to become mandatory as we move forward. As an added benefit, they provide a venue for collab-
622 orators to learn about the large scientific program for the AMBER experiment.

Presentation to Conferences:

- 12 presentations to Conferences and Workshops in 2021;
- 10 presentations to Conferences or Workshops in 2022, till May 26.

References

[1] B. Adams et al. COMPASS++/AMBER: Proposal for Measurements at the M2 beam line of the CERN SPS Phase-1: 2022-2024. Technical report, CERN, Geneva (May, 2019). URL https://cds.cern.ch/record/2676885. The collaboration has not yet constituted itself, thus instead of a Spokesperson currently the nominated Contact Person is acting in place.

[2] Minutes of the 136th Meeting of the SPSC, Tuesday and Wednesday, 21-22 January 2020. Technical report, CERN, Geneva (Jan, 2020). URL https://cds.cern.ch/record/2706935.

[3] Minutes of the 235th meeting of the Research Board, held on 2 December 2020. Technical report, CERN, Geneva (Dec, 2020). URL https://cds.cern.ch/record/2746325.

[4] J. Bernhard et al. Studies for new experiments at the CERN M2 beamline within "physics beyond colliders": AMBER/COMPASS++, NA64μ, MuonE. In *Proceedings of the 15th international conference on meson-nucleon physics and the structure of the nucleus*. AIP Publishing, (2020). [doi:10.1063/5.0008957]. URL https://doi.org/10.1063%2F5.0008957.

[5] S. Amendolia et al., A measurement of the kaon charge radius, *Physics Letters B* **178** (1986) 435–440. ISSN 0370-2693. [doi:https://doi.org/10.1016/0370-2693(86)91407-3]. URL https://www.sciencedirect.com/science/article/pii/0370269386914073.

[6] S. Amendolia et al., A measurement of the space-like pion electromagnetic form factor, *Nuclear Physics B* **277** (1986) 168–196. ISSN 0550-3213. [doi:https://doi.org/10.1016/0550-3213(86)90437-2]. URL https://www.sciencedirect.com/science/article/pii/0550321386904372.

[7] M. Aicher, A. Schäfer, and W. Vogelsang, Soft-gluon resummation and the valence parton distribution function of the pion, *Phys. Rev. Lett.* **105** (2010) 252003. [doi:10.1103/PhysRevLett.105.252003]. URL https://link.aps.org/doi/10.1103/PhysRevLett.105.252003.

[8] P. C. Barry, N. Sato, W. Melnitchouk, and C.-R. Ji [Jefferson Lab Angular Momentum (JAM) Collaboration], First monte carlo global qcd analysis of pion parton distributions, *Phys. Rev. Lett.* **121** (2018) 152001. [doi:10.1103/PhysRevLett.121.152001]. URL https://link.aps.org/doi/10.1103/PhysRevLett.121.152001.

[9] Z.-F. Cui, M. Ding, F. Gao, K. Raya, D. Binosi, L. Chang, C. D. Roberts, J. Rodríguez-Quintero, and S. M. Schmidt, Kaon and pion parton distributions, *The European Physical Journal C* **80** (2020) 1064. [doi:10.1140/epjc/s10052-020-08578-4].

[10] Z.-F. Cui, M. Ding, F. Gao, K. Raya, D. Binosi, L. Chang, C. D. Roberts, J. Rodríguez-Quintero, and S. M. Schmidt, Higgs modulation of emergent mass as revealed in kaon and pion parton distributions, *The European Physical Journal A* **57** (2021) 5. [doi:10.1140/epja/s10050-020-00318-2].

[11] C. D. Roberts, D. G. Richards, T. Horn, and L. Chang, Insights into the emergence of mass from studies of pion and kaon structure, *Progress in Particle and Nuclear Physics* **120** (2021) 103883. ISSN 0146-6410. [doi:https://doi.org/10.1016/j.ppnp.2021.103883]. URL https://www.sciencedirect.com/science/article/pii/S0146641021000375.

[12] B. Adams et al. Letter of Intent: A New QCD facility at the M2 beam line of the CERN SPS. Technical report, CERN, Geneva (August, 2018). URL http://cds.cern.ch/record/2653603.

[13] C. Ahdida, C. M., and H. Morimoto. Compass - 2018 radiation protection survey. Technical report, CERN, Geneva (January, 2019). URL https://edms.cern.ch/document/2006094/1.

[14] C. Ahdida and H. Morimoto. Compass - 2018 radiation protection survey 2. Technical report, CERN, Geneva (May, 2019). URL https://edms.cern.ch/document/2086239/1.

[15] S. Girod. Shielding for high intensity hadron operation of M2. Technical report, CERN, Geneva (March, 2022). URL https://edms.cern.ch/document/2688172/1.

[16] A. Devienne and C. Ahdida. Presentation of RP study for Drell-Yan program. Technical report, CERN, Geneva (March, 2022). URL https://edms.cern.ch/document/2718325/1.

[17] A. Devienne and C. Ahdida. RP study for AMBER Drell-Yan program. Technical report, CERN, Geneva (March, 2022). URL https://edms.cern.ch/document/2670569/1. To be released.

[18] C. Aidala et al., The phenix forward silicon vertex detector, *Nuclear Instruments and Methods in Physics Research Section A: Accelerators, Spectrometers, Detectors and Associated Equipment* **755** (2014) 44–61. ISSN 0168-9002. [doi:https://doi.org/10.1016/j.nima.2014.04.017]. URL https://www.sciencedirect.com/science/article/pii/S0168900214004124.

[19] M. Aghasyan et al. [COMPASS Collaboration], First measurement of transverse-spin-dependent azimuthal asymmetries in the drell-yan process, *Phys. Rev. Lett.* **119** (2017) 112002. [doi:10.1103/PhysRevLett.119.112002]. URL https://link.aps.org/doi/10.1103/PhysRevLett.119.112002.

[20] L. Gatignon, D. Banerjee, J. Bernhard, M. Brugger, N. Charitonidis, G. L. D'Alessandro, N. Doble, M. Van Dijk, A. Gerbershagen, E. Montbarbon, and M. Rosenthal. Report from the Conventional Beams Working Group to the Physics beyond Colliider Study and to the European Strategy for Particle Physics. Technical report, CERN, Geneva (December, 2018). URL https://cds.cern.ch/record/2650989/. Section 4.6.

[21] S. Schuh-Erhard et al. Report from the rf-separated beams workshop of 30th september 2021. Technical report, CERN, Geneva, (2021). URL https://indico.cern.ch/event/1069879. To be published.

[22] A. Gerbershagen, V. Andrieux, J. Bernhard, M. Brugger, O. Denisov, J. Friedrich, L. Gatignon, F. Gerigk, A. Guskov, B. Ketzer, F. Metzger, W.-D. Nowak, C. Quintans, and S. Schuh-Erhard, RF-Separated Beam Project for the M2 Beam Line at CERN, (2022). URL http://cds.cern.ch/record/2806692.

[23] J. Badier et al., Measurement of the k^- π^- structure function ratio using the drell-yan process, *Physics Letters B* **93** (1980) 354–356. ISSN 0370-2693. [doi:https://doi.org/10.1016/0370-2693(80)90530-4]. URL https://www.sciencedirect.com/science/article/pii/0370269380905304.

[24] H.-W. Lin, J.-W. Chen, Z. Fan, J.-H. Zhang, and R. Zhang, Valence-quark distribution of the kaon and pion from lattice qcd, *Phys. Rev. D* **103** (2021) 014516. [doi:10.1103/PhysRevD.103.014516]. URL https://link.aps.org/doi/10.1103/PhysRevD.103.014516.

[25] W. S. et al. CEDAR PID using the Likelihood Approach for the Hadron-Beam. Technical report, CERN, Geneva, (2017). URL https://wwwcompass.cern.ch/compass/notes_public/2017-1.pdf.

[26] F. Metzger et al. Conventional Hadron Beam Optimization. Technical report, CERN, Geneva, (2022). URL https://indico.cern.ch/event/1133376/contributions/4786345/attachments/2414779/4131879/AMBER_Workshop.pdf.

[27] D. Impiombato, S. Giarrusso, T. Mineo, O. Catalano, C. Gargano, G. La Rosa, F. Russo, G. Sottile, S. Billotta, G. Bonanno, S. Garozzo, A. Grillo, D. Marano, and G. Romeo, Characterization and performance of the asic (citiroc) front-end of the astri camera, *Nuclear Instruments and Methods in Physics Research Section A: Accelerators, Spectrometers, Detectors and Associated Equipment* **794** (2015) 185–192. ISSN 0168-9002. [doi:https://doi.org/10.1016/j.nima.2015.05.028]. URL https://www.sciencedirect.com/science/article/pii/S0168900215006609.

[28] T. Pöschl, D. Greenwald, M. J. Losekamm, and S. Paul, Measurement of ionization quenching in plastic scintillators, *Nuclear Instruments and Methods in Physics Research Section A: Accelerators, Spectrometers, Detectors and Associated Equipment* **988** (2021) 164865. ISSN 0168-9002. [doi:10.1016/j.nima.2020.164865]. URL http://dx.doi.org/10.1016/j.nima.2020.164865.

[29] M. Losekamm, M. Milde, T. Pöschl, D. Greenwald, and S. Paul, A new analysis method using bragg curve spectroscopy for a multi-purpose active-target particle telescope for radiation monitoring, *Nuclear Instruments and Methods in Physics Research Section A: Accelerators, Spectrometers, Detectors and Associated Equipment* **845** (2017) 520–523. ISSN 0168-9002. [doi:https://doi.org/10.1016/j.nima.2016.05.029]. URL https://www.sciencedirect.com/science/article/pii/S0168900216303953. Proceedings of the Vienna Conference on Instrumentation 2016.

[30] G. Aglieri Rinella, The alpide pixel sensor chip for the upgrade of the alice inner tracking system, *Nuclear Instruments and Methods in Physics Research Section A: Accelerators, Spectrometers, Detectors and Associated Equipment* **845** (2017) 583–587. ISSN 0168-9002. [doi:https://doi.org/10.1016/j.nima.2016.05.016]. URL https://www.sciencedirect.com/science/article/pii/S0168900216303825. Proceedings of the Vienna Conference on Instrumentation 2016.

[31] G. De Robertis, G. Fanizzi, F. Loddo, V. Manzari, and M. Rizzi, A MOdular System for Acquisition, Interface and Control (MOSAIC) of detectors and their related electronics for high energy physics experiment, *EPJ Web Conf.* **174** (2018) 07002. 4 p. [doi:10.1051/epjconf/201817407002]. URL https://cds.cern.ch/record/2314957.

[32] V. Frolov, S. Huber, I. Konorov, A. Kveton, D. Levit, J. Novy, D. Steffen, B. M. Veit, M. Virius, M. Zemko, and S. Paul, Data Acquisition System for the COMPASS++/ AMBER Experiment, *IEEE Trans. Nucl. Sci.* **68** (2021) 1891–1898. 8 p. [doi:10.1109/tns.2021.3093701]. URL https://cds.cern.ch/record/2778915.